

# The Magnetospheric Eternally Collapsing Object (MECO) Model of Galactic Black Hole Candidates and Active Galactic Nuclei

Stanley L. Robertson\* and Darryl J. Leiter†

## Abstract

The spectral, timing, and jet formation properties of neutron stars in low mass x-ray binary systems are influenced by the presence of central magnetic moments. Similar features shown by the galactic black hole candidates (GBHC) strongly suggest that their compact cores might be intrinsically magnetic as well. We show that the existence of intrinsically magnetic GBHC is consistent with a new class of solutions of the Einstein field equations of General Relativity. These solutions are based on a strict adherence to the Strong Principle of Equivalence (SPOE) requirement that the world lines of physical matter must remain timelike in all regions of spacetime. The new solutions emerge when the structure and radiation transfer properties of the energy momentum tensor on the right hand side of the Einstein field equations are appropriately chosen to dynamically enforce this SPOE requirement of timelike world line completeness. In this context, we find that the Einstein field equations allow the existence of highly red shifted, Magnetospheric, Eternally Collapsing Objects (MECO). MECO necessarily possess intrinsic magnetic moments and they do not have trapped surfaces that lead to event horizons and curvature singularities. Their most striking features are equipartition magnetic fields, pair plasma atmospheres and extreme gravitational redshifts. Since MECO lifetimes are orders of magnitude greater than a Hubble time, they provide an elegant and unified framework for understanding a broad range of observations of GBHC and active galactic nuclei. We examine their spectral, timing and jet formation properties and discuss characteristics that might lead to their confirmation.

## 1 Introduction

The evidence for the existence of massive objects that are compact enough to be black holes is strong, although there is as yet no direct evidence of any mass that is contained within its Schwarzschild radius. Supermassive compact objects have been found in the nuclei of most galaxies, while objects of stellar mass are abundant

---

\*Dept. of Physics, Southwestern Oklahoma State University, Weatherford, OK 73096

†MARC, P.O. 7466, Charlottesville, VA 22901

within our own and other galaxies. They are commonly called black holes nowadays, though no compelling evidence of an event horizon, the quintessential feature of a black hole, has yet been found. It is true that in quiescent states of galactic black hole candidates (GBHC) there are no thermal soft x-ray emission peaks, such as those possibly seen in some neutron star (NS) systems. These less luminous x-ray emissions of quiescent GBHC compared to quiescent NS have been attributed to the presence of an event horizon [Narayan, Garcia & McClintock 1997], but not compellingly so [Abramowicz, Kluzniak & Lasota 2002]. Although no thermal peak has been discerned for quiescent GBHC, both GBHC and NS systems produce power-law soft x-ray spectra of photon index  $\sim 1.7$  or softer for lower luminosities. We show that these emissions from quiescent NS systems are clearly magnetospheric in origin. In the magnetic, eternally collapsing object (MECO) model of BHC which we explore here, the similar quiescent spectra of GBHC originate in the same way, but at lower luminosity due, primarily, to slower rates of spin for the GBHC. For a given magnetic moment, the radiation rate depends on the fourth power of the spin frequency. The MECO model is fully compatible with General Relativity.<sup>1</sup> The great strength of the MECO model is that it allows a unified description of all of the various spectral, luminosity, and rapid variability states of x-ray novae, whether NS or GBHC. We show that it can be extended also to the realm of active galactic nuclei (AGN). In following sections and appendixes we provide the general relativistic theoretical basis for the existence of MECO, describe their physical characteristics, their interactions with accretion disks, their abilities to power jets and describe how the various spectral states are related to the MECO - magnetosphere - disk interactions. To avoid interrupting the presentation of ideas that are closely tied to observational issues, we have placed several separate topics in the appendixes and have referred to them as needed. The details in Appendix D are central to our understanding of the physics that dictates the large redshifts of the MECO model. The radiating MECO model is necessarily described by the Vaidya metric, for which there is no transformation to the Kerr-Schild coordinates used in many black hole models.

## 2 The Case for Intrinsic, Central Magnetic Moments:

The similarities of NS and GBHC properties, particularly in low and quiescent states, have been previously noted, [e.g. van der Klis 1994, Tanaka & Shibazaki 1996]. Jets and their synchrotron emissions in NS, GBHC and AGN also have obvious magnetic signatures. It is axiomatic that astrophysical objects of stellar mass and beyond have magnetic moments if they are not black holes, but an intrinsic magnetic moment is not a permissible attribute of a black hole. Yet in earlier work, [Robertson & Leiter 2002] we presented evidence for the existence of intrinsic mag-

---

<sup>1</sup>.. and perhaps other gravitational theories; the prime requirement being that objects with extremely large gravitational redshifts be encompassed by the theory.

netic moments of  $\sim 10^{29-30}$  gauss cm<sup>3</sup> in the GBHC of LMXB. These findings are recapitulated and extended in Table 1 and Appendix C. Calculated values in Table 1 (see also Section 8) have been corrected using a more recent correlation of spin-down energy loss rate and soft x-ray luminosity [Possenti et al. 2002], but results are scarcely changed from the previous work [Robertson & Leiter 2002] except for new additions listed in bold font. Observational luminosity and spectral data were analyzed to obtain magnetic moments and spins of the objects in the table. These magnetic moments and spin rates were then used to predict quiescent luminosities  $\sim 10^{3-6}$  times less luminous than those analyzed. The accurate predictions of quiescent luminosities and predicted spin rates comparable to those observed in NS burst oscillations [Strohmayer & Markwart 2002, Chakrabarty et al. 2003] are very powerful confirmation of the magnetospheric origin of quiescent power-law luminosity. The magnetic moments are reassuringly similar in magnitude to those determined from the spin-down rates of similarly rotating millisecond pulsars. Combined with rotation rates in the range 1 - 40 Hz, the GBHC magnetic moments provide a robust unified mechanism for the X-ray spectral state switches observed in GBHC and NS, a common origin of quiescent power-law emissions as spin-down luminosity, and a unified driving mechanism for the ubiquitous low-state jets and synchrotron emissions of both. We have shown [Robertson & Leiter 2004 and Section 10] that the jet mechanism scales up to the AGN without difficulty. Magnetosphere topology also serves to stabilize the inner accretion disk in LMXB [Arons et al. 1984].

There is a plethora of piece meal models of the various spectral and timing characteristics of LMXB. For example, comptonizing coronae near event horizons, bulk flow comptonization and magnetic flares on accretion disks have all been invoked to explain the hard spectral tail of low state GBHC. But the observed ingress/egress times for dipping sources imply large radiating regions [Church 2001] that are inconsistent with the compact corona models and can be consistent with bulk comptonization models only for large scale outflows. Similarly, radiatively inefficient advective accretion flows (ADAF) at high accretion rates have been proposed to explain the quiescent power-law emissions of GBHC, [Narayan et al. 1997, Garcia et al. 2001], while ignoring the fact that we have explained the similar emissions of accreting millisecond pulsars and the NS of LMXB via magnetospheric spin-down. It is also very disconcerting that ADAF models are clearly excluded for NS systems. The ADAF accretion rates are so high that the only way to accommodate them would be to have a very efficient magnetic propeller mechanism to prevent the flow from reaching the NS surface and producing very non-quiescent levels ( $10^{35-36}$  erg/s) of emission. But if a magnetic propeller expels a low-state ADAF flow, then quiescent NS would necessarily be extremely strong radio sources, contrary to observations.

Stating the similarities of GBHC and NS systems more bluntly, Cir X-1, a burster and a ‘Z track’ source with a magnetic moment similar to those we have found for GBHC [Table 1 and Iaria et al. 2001], exhibits all of the x-ray spectral and timing characteristics that have been proposed at various times as distinguishing features

Table 1: <sup>a</sup>Calculated and Observed Quiescent Luminosities

Object	m M <sub>⊙</sub>	$L_{min}$ 10 <sup>36</sup> erg/s	$L_c$ 10 <sup>36</sup> erg/s	$\mu_{27}$ Gauss cm <sup>3</sup>	$\nu_{obs}$ Hz obs.	$\nu_{calc}$ Hz calc.	log ( $L_q$ ) erg/s obs.	log ( $L_q$ ) erg/s calc.
<b>NS</b>								
Aql X-1	1.4	1.2	0.4	0.47	549	658	32.6	32.5
4U 1608-52	1.4	10	2.9	1.0	619	534	33.3	33.4
Sax J1808.4-3658	1.4	<sup>b</sup> 0.8	0.2	0.53	401	426	31.8-32.2	32
Cen X-4	1.4	4.4	1.1	1.1		430	32.4	32.8
KS 1731-26	1.4		1.8	1.0	524		<sup>c</sup> <b>32.8</b>	33.1
<b>XTE J1751-305</b>	1.4		3.5	1.9	435		<34.3	33.7
<b>XTE J0929-314</b>	1.4		4.9	8.5	185			33.1
4U 1916-053	1.4	~14	3.2	3.7	270	370		33.0
<b>4U1705-44</b>	1.4	26	7	2.5		470		33.7
4U 1730-335	1.4	10		2.5	307			32.9
<b>GRO J1744-28</b>	1.4		18	13000	2.14			31.5
Cir X-1	1.4	300	14	170		35		32.8
<b>GBHC</b>								
GRS 1124-68	5	240	6.6	720		16	< 32.4	32.7
GS 2023+338	7	1000	48	470		46	33.7	34
XTE J1550-564	7	<sup>d</sup> 90	4.1	150		45	32.8	32.2
GS 2000+25	7		0.15	160		14	30.4	30.5
GRO J1655-40	7	31	1.0	250		19	31.3	31.7
A0620-00	4.9	4.5	0.14	50		26	30.5	30.2
Cygnus X-1	10		30	1260		23		33
GRS 1915+105	7		12	273	<sup>e</sup> 27			33
<b>XTE J1118+480</b>	7		1.2	1000		8		31.5
<b>LMC X-3</b>	7	600	7	860		16		33

<sup>a</sup>New table entries in bold font are described in Appendix C.

Equations used for calculations of spins, magnetic moments and  $L_q$  are in Section 8

Other tabular entries and supporting data are in Robertson & Leiter [2002]

<sup>b</sup>2.5 kpc, <sup>c</sup> [Burderi et al. 2002], <sup>d</sup>d = 4 kpc

<sup>e</sup>GRS 1915+105 Q  $\approx$  20 QPO was stable for six months and a factor of five luminosity change.

of black holes. Both Cir X-1 and Cygnus X-3, a pulsar microquasar, [Brazier et al. 1990, Mitra 1998] are strong jet and radio sources similar to GBHC Cygnus X-1 and GX 339-4. A unified model of GBHC and NS is clearly needed. It is difficult to understand how such common behaviors of obviously magnetic origin could be produced both with and without event horizons.

Others have reported evidence for strong magnetic fields in GBHC. A field in excess of  $10^8$  G has been found at the base of the jets of GRS 1915+105 [Gliozzi, Bodo & Ghisellini 1999, Vadawale, Rao & Chakrabarti 2001]. A recent study of optical polarization of Cygnus X-1 in its low state [Gnedin et al. 2003] has found a slow GBHC spin and a magnetic field of  $\sim 10^8$  gauss at the location of its optical emission. These field strengths exceed disk plasma equipartition levels, but given the  $r^{-3}$  dependence of field strength on magnetic moment, the implied magnetic moments are in very good agreement with those we report in Table 1. A recent correlation [Mauche et al. 2002, Warner & Woudt 2003] of quasi-periodic oscillation (QPO) frequencies extending over six orders of magnitude in frequency, from dwarf novae to neutron stars shows points for GBHC squarely in the middle of the correlation line. If the higher of the correlated frequencies is generated where the inner radius of an accretion disk interacts with a magnetosphere [Goodson, Bohm & Winglee 1999, Titarchuk & Wood 2002], this would be additional evidence of intrinsic magnetic moments for GBHC. A relativistic frame-dragging explanation of these QPO is surely not applicable.

Although there are widely studied models for generating magnetic fields in accretion disks, they can produce equipartition fields at best [Livio, Ogilvie & Pringle 1999], and perhaps at the expense of being too luminous [Bisnovatyi-Kogan & Lovelace 2000] in quiescence and in any case, too weak and comoving in accretion disks to drive jets. While tangled magnetic fields in accretion disks are very likely responsible for their large viscosity, [e.g. Hawley, Balbus & Winters 1999] the highly variable mass accretion rates in LMXB make it unlikely that disk dynamos could produce the stability of fields needed to account for either spectral state switches or quiescent spin-down luminosities. Both require magnetic fields co-rotating with the central object. Further, if disk dynamos produced the much larger apparent magnetic moments of GBHC, they should produce them also for the NS systems and cause profound qualitative spectral and timing differences from GBHC due to interactions with the intrinsic NS magnetic moments. Such qualitative differences as have been observed, e.g., the hard spectral tail of the steep power law (intermediate) state, lack of surface bursts for GBHC and stronger GBHC jets, (excepting NS Cir X-1 and Cygnus X-3) are easily explained by differences in masses, magnetic field strengths and surface redshift. Not only are there are no observed differences that require explanation in terms of event horizons [Abramowicz, Kluzniak & Lasota 2002], there appear to be none that would be consistent with having two different magnetic structures for NS and only one GBHC.

It has been suggested that stable magnetic fields could be produced by electri-

cally charged, rotating black holes [Punsly 1998, Gnedin et al. 2003], however the charge necessary to endow Cygnus X-1 with a  $10^8$  G magnetic field, well out in the accretion disk, was found to be  $5 \times 10^{28}$  esu [Gnedin et al. 2003]. Due to the large charge/mass ratios of accreting protons or electrons, this quantity of charge on a black hole would produce electric forces at least  $\sim 10^6$  larger than the gravitational attraction of a  $10M_{\odot}$  GBHC, thus causing charges of one sign to be swallowed and the other to be blown away. At accretion rates needed to account for the x-ray luminosity of Cygnus X-1, the original charge would be neutralized in a fraction of one second. Thus it appears that current black hole models are unable to offer unified explanations of such obviously magnetic phenomena as jets, spectral state switches and quiescent synchrotron emissions and if they could, it seems unusually generous for nature to have provided different mechanisms by which NS and GBHC could produce such strikingly similar phenomena.

In Table 1, we have provided solid evidence for the applicability of a spinning magnetic moment model of LMXB and we have presented reasons for considering these magnetic moments to be intrinsic to the central object rather than being generated within an accretion disks. While accommodating intrinsic magnetic moments in models of GBHC will require abandoning the currently popular black hole theory of GBHC, it will also greatly simplify the problem of understanding the spectral, timing and jet ejection mechanisms of compact objects. As noted by Abramowicz, Kluzniak & Lasota [2002], it is unlikely that we will ever find direct observational proof of an event horizon, however, we may be able to definitively determine whether or not GBHC have intrinsic magnetic moments. We regard Table 1 as strongly suggestive, if not yet definitive. If GBHC are not black holes, they would almost certainly be magnetized, and likely to at least a degree similar to their compact NS cousins.

In our MECO model, we have found that it is possible to virtually stop and maintain a slow, (many Hubble times!) steady collapse of a compact physical plasma object outside of its Schwarzschild radius with photon pressure generated by synchrotron radiation from an equipartition surface magnetic field. To control the rate of collapse, the object must radiate at the local Eddington limit, but from a highly redshifted surface. (see Appendices D and E.) There is recent evidence for the presence of such extreme magnetic fields in gravitational collapse. Equipartition magnetic fields have been implicated as the driver of GRB 021206 [Coburn & Boggs 2003] and fields much in excess of those expected from mere flux compression during stellar collapse have been found in magnetars [Ibrahim, Swank & Parke 2003]. Kluzniak and Ruderman [1998] have described the generation of  $\sim 10^{17}$  G magnetic fields via differential rotation in neutron stars. In Appendix D, we show that surface drift currents within a pair plasma at the MECO surface generate its required fields. Drift currents proportional to  $\mathbf{g} \times \mathbf{B}/B^2$  occur for plasmas at rest in gravitational and magnetic fields.

The equatorial poloidal magnetic field needed for a stable rate of collapse of the

exterior surface is  $\sim 10^{20}$  gauss. Fields of this magnitude are strong enough to create bound electron-positron pairs out of the quantum electrodynamic vacuum. This assures sufficient photon pressure from annihilation radiation to stabilize the collapse rate. The magnetic field of the interior is approximately what one would expect from flux compression during collapse,  $\sim 2.5 \times 10^{13} \sqrt{7M_{\odot}/M}$  gauss and its radial component is continuous across the surface boundary. The poloidal field is discontinuous across the surface and much stronger externally due to the surface drift currents. As shown in Appendix D, at the MECO surface radius  $2R_g = 2GM/c^2$ , the ratio of poloidal field on the surface to the poloidal field just under the MECO surface is given by

$$B_{\theta,S+}/B_{\theta,S-} = (1 + z_s)/(2\ln(1 + z_s)) = 10^{20}/(2.5 \times 10^{13})\sqrt{7M_{\odot}/M} \quad (1)$$

where  $z_s$  is the surface redshift. This has the solution

$$1 + z_s = 1.5 \times 10^8 \sqrt{M/7M_{\odot}} \quad (2)$$

The distantly observed field is reduced by a surface redshift of by a factor of  $3(1 + z_s) = 4.5 \times 10^8 \sqrt{M/7M_{\odot}}$  to a level which agrees well with the observed magnetic moments shown in Table 1. The surface luminosity is reduced below the conventional Newtonian Eddington limit by  $(1 + z_s)$  when distantly observed, and the decay lifetime is extended by the same factor.

### 3 The Strong Principle of Equivalence

Astrophysicists nowadays generally accept the inevitability of the curvature singularities of black holes <sup>2</sup>, however, if the GBHC are confirmed as intrinsically magnetized, this will be nature's way of telling us that such singularities are not really permitted to exist. For black holes to exist, gravity must be able to do what no other force of nature can do; namely, to accelerate the physical three-speed of a finite mass to exactly the speed of light. But this means that horizon crossing geodesics, in realistic coordinates, would become null rather than timelike. In General Relativity (GR) the Strong Principle of Equivalence (SPOE) requires that Special Relativity (SR) must hold locally for all time-like observers in all of spacetime. This SPOE requirement is a tensor relationship that implies that (i) the spacetime manifold for observers located in field-free regions, distant from gravitating masses, must

---

<sup>2</sup>The modern notion of a black hole began with Hilbert's error of application of boundary conditions for the solutions of Einstein's field equations of General Relativity for a mass point. Hilbert's solution has been erroneously attributed to Schwarzschild, however Schwarzschild's preceding original solution had no event horizon. [see Abrams 1979, 1989] Nevertheless, Hilbert's solution is analytically extendible through the horizon to a central singularity, hence the modern black hole. The fact that the radius of the event horizon, which is directly proportional to the gravitational mass, can be changed arbitrarily by (generally singular) coordinate transformation strongly suggests that the horizon is unphysical.

approach the flat spacetime of SR <sup>3</sup> and (ii) the spacetime world lines of massive matter must always be timelike. <sup>4</sup> Such spacetime manifolds are known as ‘bundle complete’ [Wheeler & Ciufolini 1995].

As a guiding principle, we look for solutions of the Einstein equations

$$G^{\mu\nu} = (8\pi G/c^4)T^{\mu\nu} \quad (3)$$

that satisfy the SPOE requirement for timelike world line completeness. Since there is nothing in the Einstein tensor  $G^{\mu\nu}$  that enforces this condition, we must rely on non-gravitational forces in  $T^{\mu\nu}$  to dynamically enforce it. Since the energy-momentum tensor  $T^{\mu\nu}$  serves as both a source of curvature in the Einstein equations and a generator of the equations of motion of matter, constraints on  $T^{\mu\nu}$  that enforce timelike world line completeness can also eliminate the occurrence of event horizons. Thus the SPOE requires that the right hand side of the GR field equation must contain non-gravitational elements capable of stopping the collapse of physical matter before the formation of a ‘trapped surface’. This dynamically escapes the Hawking and Penrose theorem which states that once a trapped surface is formed, an event horizon and curvature singularities are unavoidable.

We can show how the SPOE constrains the solutions of the Einstein field equations. Consider a comoving interior metric given by

$$ds^2 = A(r, t)^2 c^2 dt^2 - B(r, t)^2 dr^2 - R(r, t)^2 (d\theta^2 + \sin^2\theta d\phi^2) \quad (4)$$

and an exterior Vaidya metric with outgoing radiation

$$ds^2 = (1 - 2GM/c^2 R)c^2 du^2 + 2cdudR - R^2(d\theta^2 + \sin^2\theta d\phi^2) \quad (5)$$

where  $R$  is the areal radius and  $u = t - R/c$  is the retarded observer time. Following Lindquist, Schwarz & Misner [1965], we define

$$\Gamma = \frac{dR}{dl} \quad (6)$$

---

<sup>3</sup>This eliminates Kruskal-Szekeres coordinates from the real world of astrophysics.

<sup>4</sup>Models of gravitational collapse that lead to the development of event horizons and central curvature singularities inevitably abandon the SPOE requirement for timelike world line completeness. The vanishing of the metric time coefficient,  $g_{tt}$ , at the Schwarzschild radius is sufficient to cause the timelike physical three-speed of particles in radial free fall to approach the speed of light there. In obvious notation, [Landau & Lifshitz 1975].  $V^2 = (\frac{dl}{d\tau_s})^2 = c^2 \frac{(g_{tr}g_{tr} - g_{rr}g_{tt})v^r v^r}{(g_{tt} + g_{tr}v^r)^2}$  where  $v^r = \frac{dr}{d\tau}$ . In non-singular Finkelstein or Kerr-Schild coordinates, for which  $g_{tr} \neq 0$ , we find  $V \rightarrow c$  as  $g_{tt} \rightarrow 0$ . It has been shown [Leiter & Robertson 2003] that  $ds^2 \rightarrow 0$  at surfaces of infinite redshift. In Kruskal-Szekeres coordinates, in which  $g_{tt}$  does not vanish, there is no surface of infinite redshift at the Schwarzschild radius,  $R = 2GM/c^2$ , and timelike test particle geodesics can traverse it *in either direction*, so long as the initial conditions are chosen in a manner that permits the ‘time’ coordinate to change in a positive sense. However, a central singularity still exists in these coordinates and they have a surface of infinite redshift as  $r \rightarrow \infty$ , at which  $ds^2 \rightarrow 0$ . This is an extreme example of a coordinate transformation changing the size of the event horizon radius.

$$U = \frac{dR}{d\tau} \quad (7)$$

$$M(r, t) = 4\pi \int_0^r \rho R^2 \frac{dR}{dr} dr \quad (8)$$

$$\Gamma^2 = \left(\frac{dR}{dl}\right)^2 = 1 - \frac{2GM(r, t)}{c^2 R} + \frac{U^2}{c^2} \quad (9)$$

where  $dl$  is a proper length element in a zero angular momentum comoving frame,  $d\tau$  an increment of proper time,  $U$  is the proper time rate of change of the radius associated with the invariant circumference of the collapsing mass, and  $M(r, t)$  is the mass enclosed within this radius. The last two of the relations above have been obtained from the  $G_0^0$  component of the field equation [Lindquist, Schwarz & Misner 1965]. At the boundary of the collapsing, radiating surface,  $s$ , we find that the proper time will be positive definite, as required for timelike world line completeness if

$$d\tau_s = \frac{du}{1 + z_s} = du \left(1 - \frac{2GM(r, t)_s}{c^2 R_s} + \frac{U_s^2}{c^2}\right)^{1/2} + \frac{U_s}{c} > 0 \quad (10)$$

where  $z_s$  is the distantly observed redshift of the collapsing surface. From Eq. (10) we see that in order to avoid a violation of the requirement of timelike world line completeness for  $U_s < 0$ , it is necessary to dynamically enforce the ‘no trapped surface condition’.<sup>5</sup>

$$\frac{2GM_s}{c^2 R_s} < 1 \quad (11)$$

## 4 A Radiating, Collapsing, Magnetic Object

The simplest form of the energy-momentum tensor that can satisfy the SPOE requirement of timelike world line completeness, is one that describes a collapsing, radiating plasma with an equipartition magnetic field that emits outgoing radiation. Between the extremes of pure magnetic energy [Thorne 1965] and weakly magnetic, radiation dominated polytropic gases or pressureless dust [Baumgarte & Shapiro 2003] there are cases where the rate of collapse can be stable. To first order, in an Eddington limited radiation dominated context, these can be described by the energy momentum tensor:

$$T_\mu^\nu = (\rho + P/c^2)u_\mu u^\nu - P\delta_\mu^\nu + E_\mu^\nu \quad (12)$$

---

<sup>5</sup>It might be argued that there might not be a surface that physically divides matter from radiation inside a collapsing massive continuum, however, it was first shown by Mitra [Mitra 2000, 2002] and later corroborated by Leiter & Robertson [2003] that Eq.s (7 - 9) and the  $G_0^0$  field equation in a zero angular momentum comoving frame produces the ‘no trapped surface condition’ for any interior  $R(r, t)$ . For the MECO, timelike world line completeness is maintained by photon pressure generated by the equipartition magnetic field everywhere in the comoving frame. We can consider any interior location and the radiation flux there without requiring a joined Vaidya metric. But there will ultimately be an outer radiating boundary and the required match to the non-singular outgoing exterior Vaidya metric guarantees that there will be no metric singularity there.

where  $E_\mu^\nu = Qk_\mu k^\nu$ ,  $k_\mu k^\mu = 0$  describes outgoing radiation in a geometric optics approximation,  $\rho$  is energy density of matter and  $P$  the pressure.<sup>6</sup> Here  $Q$  is given by

$$Q = \frac{-(dM/du)/4\pi R^2}{(\Gamma_s + U_s/c)^2} \quad (13)$$

At the comoving MECO surface the luminosity is

$$L = 4\pi R^2 Q > 0. \quad (14)$$

and the distantly observed luminosity is

$$L_\infty = -c^2 \frac{dM_s}{du} = -c^2 \frac{dM_s}{d\tau(1+z_s)} \quad (15)$$

After examining the relations between surface and distantly observed luminosities, we will use this relation to determine the MECO lifetime.

## 5 Eddington Limited MECO

Among the various equations associated with the collapse process there are three proper time differential equations applicable to a compact collapsing and radiating physical surface. When evaluated on the physical surface [Hernandez Jr. & Misner, 1966, Lindquist, Schwartz & Misner 1965, Misner 1965, Lindquist, 1966] these equations are:

$$\frac{dU_s}{d\tau} = \left(\frac{\Gamma^2}{\rho + P/c^2}\right)_s \left(-\frac{\partial P}{\partial R}\right)_s - \left(\frac{G(M + 4\pi R^3(P + Q)/c^2)}{R^2}\right)_s \quad (16)$$

$$\frac{dM_s}{d\tau} = -(4\pi R^2 P c \frac{U}{c})_s - (L(\frac{U}{c} + \Gamma))_s \quad (17)$$

$$\frac{d\Gamma_s}{d\tau} = \frac{G}{c^4} \left(\frac{L}{R}\right)_s + \frac{U_s}{c^2} \left(\frac{\Gamma^2}{\rho + P/c^2}\right)_s \left(-\frac{\partial P}{\partial R}\right)_s \quad (18)$$

In Eddington limited steady collapse, the conditions  $dU_s/d\tau = 0$  and  $U_s \approx 0$  hold after some time,  $\tau_{Edd}$ , that has elapsed in reaching the Eddington limited state. Then

$$\frac{dU_s}{d\tau} = \frac{\Gamma_s^2}{(\rho + P/c^2)_s} \left(-\frac{\partial P}{\partial R}\right)_s - \frac{GM_s}{R_s^2} = 0 \quad (19)$$

Where

$$M_s = (M + 4\pi R^3(P + Q)/c^2)_s \quad (20)$$

---

<sup>6</sup>Energy momentum tensors corresponding to metrics describing ingoing radiation, which are used in many black hole model calculations, (e.g. Baumgarte & Shapiro [2003]) cannot be used here because they are incompatible with the  $Q > 0$  boundary conditions associated with collapsing, outwardly radiating objects.

includes the magnetic field energy in the pressure term and radiant energy in Q.

Eq. (19) when integrated over a closed surface can be solved for the net outward flow of Eddington limited luminosity through the surface. Taking the escape cone factor of  $27(R_g/R_s)^2/(1+z_s)^2$  into account, where  $R_g = GM/c^2$ , (See Appendix A) the outflowing (but not all escaping) surface luminosity, L, would be

$$L_{Edd}(outflow)_s = \frac{4\pi GM_s c R^2 (1+z_{Edd})^3}{27\kappa R_g^2} \quad (21)$$

where  $\kappa \approx 0.4 \text{ cm}^2/g$  is the plasma opacity. (For simplicity, we have assumed here that the luminosity actually escapes from the MECO surface rather than after conveyance through a MECO atmosphere and photosphere. The end result is the same for distant observers.) However the luminosity  $L_s$  which appears in Eq.s (16 - 20) is actually the net luminosity, which escapes through the photon sphere, and is given by  $L_s = L_{Edd}(escape)_s = L_{Edd}(outflow) - L_{Edd}(fallback) = L_{Edd,s} - L_{Edd,s}(1 - 27R_g^2/(R(1+z_{Edd}))^2)$  Thus in Eq.s (17) and (18), the  $L_s$  appearing there is given by

$$L_s = L_{Edd}(escape)_s = \frac{4\pi GM(\tau)_s c (1+z_{Edd})}{\kappa} \quad (22)$$

In this context from Eq.s (9), (10), (17) and (22) we have

$$c^2 \frac{dM_s}{d\tau} = -\frac{L_{Edd}(escape)_s}{(1+z_s)} = -\frac{4\pi GM(\tau)_s c}{\kappa} \quad (23)$$

which can be integrated to give

$$M_s(\tau) = M_s(\tau_{Edd}) \exp((-4\pi G/\kappa c)(\tau - \tau_{Edd})) \quad (24)$$

This yield a distantly observed MECO lifetime of  $(1+z_s)\kappa c/4\pi G \sim 5 \times 10^{16}$  yr for  $z_s \sim 10^8$ . Finally, equation (18) becomes

$$\frac{d\Gamma_s}{d\tau} = \frac{G}{c^4} \frac{L_{Edd,s}}{R_s(\tau_{Edd})} \quad (25)$$

which, in view of (13) has the solution

$$\Gamma_s(\tau) = \frac{1}{1+z_s(\tau)} = (1 - \frac{2GM_s(\tau_{Edd})}{c^2 R_s(\tau)_{Edd}})^{1/2} > 0 \quad (26)$$

which is consistent with Eq.s (9) and (11).

If one naively attributes Eddington limit luminosity to purely thermal processes, one quickly finds that the required MECO surface temperatures would be so high that photon energies would be far beyond the pair production threshold and the compactness would assure that photon-photon collisions would produce numerous electron-positron pairs. Thus the MECO surface region must be dominated by a

pair plasma. Pelletier & Marcowith [1998] have shown that the energy density of magnetic perturbations in equipartition pair plasmas is preferentially converted to photon pressure, rather than causing particle acceleration. The radiative power of an equipartition pair plasma is proportional to  $B^4$ , (pair density  $\propto B^2$  and synchrotron energy production  $\propto B^2$ .) Lacking the equipartition pair plasma, magnetic stress,  $B^2/8\pi$ , and gravitational stress,  $GM\rho/R$ , on mass density  $\rho$ , would both increase as  $R^{-4}$  during gravitational collapse. Magnetic fields much below equipartition levels would be incapable of stopping the collapse. However, since photon pressure generated by the pairs at equipartition increases more rapidly than gravitational stresses, it is possible to stabilize the rate of collapse at an Eddington limit rate. With this extremely efficient photon-photon pair production mechanism, the radiation temperature and pressure is buffered near the pair production threshold by two types of highly redshifted quantum electrodynamic phase transitions which convert photons into pairs on the MECO surface. The first one involves optically thick photon-photon pair production while the second one occurs for MECO surface magnetic fields strong enough to create bound pairs out of the quantum electrodynamic vacuum. In the context of an Eddington limited balance generated by the former process, the latter process can lead to excess production of pairs, followed by excess photon pressure and an expansion of the MECO surface. In this manner the MECO Eddington limited collapse rate is inherently stable (see Appendix D and E). Stability is maintained by increased (decreased) photon pressure ( $\propto B^4$ ) if the field is increased (decreased) by compression or expansion. For equipartition conditions, the field also exceeds that required to confine the pair plasma. Since the photon luminosity is not confined to the core it will not be trapped, as occurs with neutrinos, however, the radiation should be thermalized as it diffuses through an optically thick environment. *To reduce the field to the distantly observed levels implied by our analysis of GBHC observations would require the existence of a red shift of  $z = 1.5 \times 10^8 (M/7M_\odot)^{1/2}$  (see Appendixes D and E).* The residual, distantly observable magnetic moment and extremely faint, redshifted radiations would be the only things that would distinguish such an object from a black hole. <sup>7</sup>

---

<sup>7</sup>An additional point of support for very large values of redshift concerns neutrino transport in stellar core collapse. If a diffusion limited neutrino luminosity of  $\sim 10^{52}$  erg/s [Shapiro & Teukolsky 1983] were capable of very briefly sustaining a neutrino Eddington limit rate of collapse, then the subsequent reduction of neutrino luminosity as neutrino emissions are depleted and trapped in the core would lead to an adiabatic collapse, magnetic flux compression, and photon emissions reaching an Eddington limit. At this point the photon luminosity would need to support a smaller diameter and more tightly gravitationally bound mass. A new photon Eddington balance would thus require an escaping luminosity reduced by at least the  $\sim 10^{20}$  opacity ratio ( $\sigma_T/\sigma_\nu$ ), where  $\sigma_T = 6.6 \times 10^{-25}$  cm<sup>2</sup> is the Thomson cross section and  $\sigma_\nu = 4.4 \times 10^{-45}$  cm<sup>2</sup> is the neutrino scattering cross-section. Thus  $L_\infty < 10^{31-32}$  erg/s would be required. For this to correspond to an Eddington limit luminosity as distantly observed would require  $1 + z \sim 10^8$ . The adiabatic relaxation of neutrino support and formation of a pair plasma is an important step in gravitational collapse that is not encompassed by polytropic equation of state models of collapse. It is of some interest that if neutrinos have non-zero rest mass they might be trapped inside the photon sphere

An electron-positron pair atmosphere of a MECO is an extremely significant structure that conveys radiation from the MECO surface to a zone with a much lower red shift and larger escape cone from which it escapes. In order to describe this process computationally within a numerical grid, a radial grid interval no larger than  $\sim 10^{-8}R_g$  would be needed, where  $R_g = GM/c^2$  is the gravitational radius. Although there have been many numerical studies of the behavior of collapsing compact objects in GR, to our knowledge none have sufficient numerical resolution to examine the extreme red shift regime associated with MECO nor have they considered the emergent properties of equipartition magnetic fields and pair plasmas at high red shift. Until computer models of gravitational collapse encompass these crucial physical and computational elements, simulations that apparently produce black hole states must be regarded as mere speculations.

## 6 The Quiescent MECO

The quiescent luminosity of a MECO originates deep within its photon sphere. When distantly observed it is diminished by both gravitational red shift and a narrow exit cone. The gravitational red shift reduces the surface luminosity by  $1/(1+z)^2$  while the exit cone further reduces the luminosity by the factor  $27R_g^2/(R(1+z))^2 \sim 27/(4(1+z)^2)$  for large  $z$ . (See Appendix A). Here we have used

$$\frac{R_g}{R} = \frac{1}{2}\left(1 - \frac{1}{(1+z)^2}\right) < \frac{1}{2} \quad (27)$$

where  $R$  and  $z$  refer to the location from which photons escape. The net outflow fraction of the luminosity provides the support for the collapsing matter, thereby dynamically maintaining the SPOE requirement of timelike world line completeness. The photons which finally escape do so from the photosphere of the pair atmosphere. The fraction of luminosity from the MECO surface that escapes to infinity in Eddington balance is

$$(L_{Edd})_s = \frac{4\pi GM_s c(1+z)}{\kappa} = 1.27 \times 10^{38} m(1+z_s) \quad \text{erg/s} \quad (28)$$

where  $m = M/M_\odot$ . The distantly observed luminosity is:

$$L_\infty = \frac{(L_{Edd})_s}{(1+z_s)^2} = \frac{4\pi GM_s c}{\kappa(1+z_s)} \quad (29)$$

When radiation reaches the photosphere, where the temperature is  $T_p$ , the fraction that escapes to be distantly observed is:

$$L_\infty = \frac{4\pi R_g^2 \sigma T_p^4 27}{(1+z_p)^4} = 1.56 \times 10^7 m^2 T_p^4 \frac{27}{(1+z_p)^4} \quad \text{erg/s} \quad (30)$$

anyway.

where  $\sigma = 5.67 \times 10^{-5}$  erg/s/cm<sup>2</sup> and subscript p refers to conditions at the photosphere. Eq.s (29) and (30) yield:

$$T_\infty = T_p/(1 + z_p) = \frac{2.3 \times 10^7}{(m(1 + z_s))^{1/4}} \quad K. \quad (31)$$

To examine typical cases, a  $10M_\odot$ ,  $m = 10$  GBHC modeled in terms of a MECO with  $z = 1.5 \times 10^8(m/7)^{1/2}$  would have  $T_\infty = 1.1 \times 10^5 K = 0.01$  keV, a bolometric luminosity, excluding spin-down contributions, of  $L_\infty = 7.3 \times 10^{30}$  erg/s, and a spectral peak at  $220 \text{ \AA}$ , in the photoelectrically absorbed deep UV. For an  $m=10^7$  AGN,  $T_\infty = 630K$ ,  $L_\infty = 7.2 \times 10^{33}$  erg/s and a spectral peak in the infrared at  $4\mu$ . (Sgr A\* at  $m \approx 3 \times 10^6$ , would have  $T_\infty = 1100$  K, and a 2.2 micron brightness below 0.6 mJy; more than an order of magnitude below the observational upper limit of 9 mJy [Reid et al. 2003].) Hence passive MECO without active accretion disks, although not black holes, have lifetimes much greater than a Hubble time and emit highly red shifted quiescent thermal spectra that may be quite difficult to observe. There are additional power law components of similar magnitude that originate as magnetic dipole spin-down radiation (Table 1 and see below).

Escaping radiation passes through a pair plasma atmosphere that can be shown, *ex post facto* (See Appendix B), to be radiation dominated throughout. In fact, at the extreme redshifts contemplated here, Mitra (2006) has shown that the interior of the collapsed object must be radiation dominated. Under these circumstances, the radiation pressure within the equilibrium atmosphere obeys  $P_{rad}/(1 + z) = \text{constant}$ <sup>8</sup>. Thus the relation between surface and photosphere temperatures is  $T_s^4/(1 + z_s) = T_p^4/(1 + z_p)$ . At the MECO surface, we expect a pair plasma temperature of  $T_s \approx m_e c^2/k \sim 6 \times 10^9 K$  because an equipartition magnetic field effectively acts as a thermostat which buffers the temperature of the optically thick synchrotron radiation escaping from the MECO surface [Pelletier & Marcowith 1998]. But since  $T_\infty = T_p/(1 + z_p)$ , and using  $T_s = 6 \times 10^9$  K, we have that

$$T_p = T_s \left( \frac{T_s}{T_\infty(1 + z_s)} \right)^{1/3} = 3.8 \times 10^{10} \frac{m^{1/12}}{(1 + z_s)^{1/4}} = 4.5 \times 10^8 (m/7)^{-1/24} \quad K \quad (32)$$

In the last expression, we have used  $1 + z_s = 1.5 \times 10^8(m/7)^{1/2}$ . Using Eq. (31), this leads immediately to  $(1 + z_p) = 3500 \times (m/7)^{1/3}$ , independent of the surface redshift, thus confirming that for MECO with pair atmospheres to exist, they must be inherently highly redshifted. Due to the very weak dependence of  $T_p$  on  $m$ , the photosphere temperatures of MECO are all very nearly  $4.5 \times 10^8$  K.

---

<sup>8</sup>Due to its negligible mass, we consider the pair atmosphere to exist external to the Meco. Due to the slow collapse, the exterior Vaidya metric can be approximated by exterior, outgoing Finkelstein coordinates. In this case, the hydrostatic balance equation within the MECO atmosphere is  $\frac{\partial p}{\partial r} = -\frac{\partial \ln(g_{00})}{2\partial r}(p + \rho c^2)$ , where  $g_{00} = (1 - 2R_g/r)$  and  $\rho c^2 \ll p$ . This integrates to  $p/(1 + z) = \text{constant}$ .

## 7 An Actively Accreting MECO

From the viewpoint of a distant observer, accretion would deliver mass-energy to the MECO, which would then radiate most of it away. The contribution from the central MECO alone would be

$$L_\infty = \frac{4\pi GM_s c}{\kappa(1+z_s)} + \frac{\dot{m}_\infty c^2}{1+z_s}(e(1+z_s) - 1) = 4\pi R_g^2 \sigma T_p^4 \frac{27}{(1+z_p)^4} \quad (33)$$

where  $e = E/mc^2 = 0.943$  is the specific energy per particle available after accretion disk flow to the marginally stable orbit radius,  $r_{ms}$ . Assuming that  $\dot{m}_\infty$  is some fraction,  $f$ , of the Newtonian Eddington limit mass accretion rate,  $4\pi GM_c/\kappa$ , then

$$1.27 \times 10^{38} \frac{m\eta}{1+z_s} = (27)(1.56 \times 10^7)m^2 \left(\frac{T_p}{1+z_p}\right)^4 \quad (34)$$

where  $\eta = 1 + f((1+z_s)e - 1)$  includes both quiescent and accretion contributions to the luminosity. Due to the extremely strong dependence on temperature of the density of pairs, (see Appendix B) it is unlikely that the temperature of the photosphere will be greatly different from the average of  $4.6 \times 10^8 K$  found previously for a typical GBHC. Assuming this to be the case, along with  $z = 10^8$ ,  $m = 10$ , and  $f = 1$ , we find  $T_\infty = T_p/(1+z_p) = 1.3 \times 10^7 K$  and  $(1+z_p) = 35$ , which indicates considerable photospheric expansion. The MECO luminosity would be approximately Newtonian Eddington limit at  $L_\infty = 1.2 \times 10^{39}$  erg/s. For comparison, the accretion disk outside the marginally stable orbit at  $r_{ms}$  (efficiency = 0.057) would produce only  $6.8 \times 10^{37}$  erg/s. Thus the high accretion state luminosity of a GBHC would originate primarily from the central MECO. The thermal component would be ‘ultrasoft’ with a temperature of only  $1.3 \times 10^7 K$  (1.1 keV). A substantial fraction of the softer thermal luminosity would be Compton scattered to higher energy in the plunging flow inside  $r_{ms}$ . Even if a disk flow could be maintained all the way to the MECO surface, where a hot equatorial band might result, the escaping radiation would be spread over the larger area of the photosphere due to photons origins deep inside the photon orbit.

For radiation passing through the photosphere most photons would depart with some azimuthal momentum on spiral trajectories that would eventually take them across and through the accretion disk. Thus a very large fraction of the soft photons would be subject to bulk comptonization in the plunging region inside  $r_{ms}$ . This contrasts sharply with the situation for neutron stars where there probably is no comparable plunging region and few photons from the surface cross the disk. This could account for the fact that hard x-ray spectral tails are comparatively much stronger for high state GBHC. Our preliminary calculations for photon trajectories randomly directed upon leaving the photon sphere indicate that this process would produce a power law component with photon index greater than 2. These are difficult, but important calculations for which the effects of multiple scattering must

be considered. But they are beyond the scope of this work, which is intended as a first description of the general MECO model.

## 8 Magnetosphere - Disk Interaction

In LMXB, when the inner disk engages the magnetosphere, the inner disk temperature is generally high enough to produce a very diamagnetic plasma. This may not be the case for AGN. Surface currents on the inner disk distort the magnetopause and they also substantially shield the outer disk such that the region of strong disk-magnetosphere interaction is mostly confined to a ring or torus, of width  $\delta r$  and half height  $H$ . This shielding leaves most of the disk under the influence of its own internal shear dynamo fields, [e.g. Balbus & Hawley 1998, Balbus 2003]. At the inner disk radius the magnetic field of the central MECO is much stronger than the shear dynamo field generated within the inner accretion disk. In MHD approximation, the force density on the inner ring is  $F_v = (\nabla \times B) \times B/4\pi$ . For simplicity, we assume coincident magnetic and spin axes of the central object and take this axis as the  $z$  axis of cylindrical coordinates  $(r, \phi, z)$ .

The magnetic torque per unit volume of plasma in the inner ring of the disk that is threaded by the intrinsic magnetic field of the central object, can be approximated by  $\tau_v = rF_{v\phi} = r\frac{B_z}{4\pi}\frac{\partial B_\phi}{\partial z} \sim r\frac{B_z B_\phi}{4\pi H}$ , where  $B_\phi$  is the average azimuthal magnetic field component. We stress that  $B_\phi$ , as used here, is an average toroidal magnetic field component. The toroidal component likely varies episodically between reconnection events [Goodson & Winglee 1999, Matt et al. 2002, Kato, Hayashi & Matsumoto 2004, Uzdensky 2002].

The average flow of disk angular momentum entering the inner ring is  $\dot{M}rv_k$ , where  $\dot{M}$  is mass accretion rate and  $v_k$  is the Keplerian speed in the disk. This angular momentum must be extracted by the magnetic torque,  $\tau$ , hence:

$$\tau = \dot{M}rv_k = r\frac{B_z B_\phi}{4\pi H}(4\pi r H \delta r). \quad (35)$$

In order to proceed further, we assume that  $B_\phi = \lambda B_z$ ,  $B_z = \mu/r^3$ , and use  $v_k = \sqrt{GM/r}$ , where  $\lambda$  is a constant, presumed to be of order unity,  $\mu$  is the magnetic dipole moment of the central object  $M$ , its mass, and  $G$ , the Newtonian gravitational force constant. With these assumptions we obtain

$$\dot{M} = \left(\frac{\lambda\delta r}{r}\right)\frac{\mu^2}{r^5\omega_k} \quad (36)$$

where  $\omega_k = v_k/r$  and the magnetopause radius,  $r_m$  is given by

$$r_m = \left(\frac{\lambda\delta r}{r}\right)^{2/7}\left(\frac{\mu^4}{GMM^2}\right)^{1/7} \quad (37)$$

In order to estimate the size of the boundary region,  $(\delta r/r)$ , we normalized this disk-magnetosphere model for agreement with radii calculated for an elaborate

model of a gas pressure dominated disk [Ghosh & Lamb 1992]. Although we find the portion of the inner disk threaded by magnetic fields to be smaller than the Ghosh & Lamb model, this size for the inner radius yields very accurate results for accreting millisecond pulsars, which have known magnetic moments. We find  $(\frac{\lambda\delta r}{r}) = 0.015$ , which indicates a gratifyingly small strong interaction zone for disk and magnetosphere. Using units of  $10^{27}$  gauss  $\text{cm}^3$  for magnetic moments, 100 Hz for spin,  $10^6$  cm for radii,  $10^{15}$  g/s for accretion rates, solar mass units,  $\lambda\delta r/r = 0.015$  and otherwise obvious notation, we find the magnetosphere radius to be:

$$r_m = 8 \times 10^6 \left( \frac{\mu_{27}^4}{m\dot{m}_{15}^2} \right)^{1/7} \text{ cm} \quad (38)$$

where  $m = M/M_\odot$  and the disk luminosity is

$$L = \frac{GM\dot{m}}{2r_m} \quad (39)$$

The co-rotation radius, at which disk Keplerian and magnetosphere spins match is:

$$r_c = 7 \times 10^6 \left( \frac{m}{\nu_2^2} \right)^{1/3} \text{ cm} \quad (40)$$

The low state disk luminosity at the co-rotation radius is the maximum luminosity of the true low state and is given by:

$$L_c = \frac{GM\dot{m}}{2r_c} = 1.5 \times 10^{34} \mu_{27}^2 \nu_2^3 m^{-1} \text{ erg/s} \quad (41)$$

The minimum high state luminosity for all accreting matter being able to reach the central object occurs at approximately the same accretion rate as for  $L_c$  and is given by:

$$L_{min} = \xi \dot{m} c^2 = 1.4 \times 10^{36} \xi \mu_{27}^2 \nu_2^{7/3} m^{-5/3} \text{ erg/s} \quad (42)$$

Where  $\xi \sim 0.42$  for MECO for the photon sphere<sup>9</sup> and  $\xi = 0.14$  for NS is the efficiency of accretion to the central surface.

In true quiescence, the inner disk radius is larger than the light cylinder radius. In NS and GBHC, the inner disk may be ablated due to radiation from the central object. The inner disk radius can be ablated to distances larger than  $5 \times 10^4 \text{ km}$  because optically thick material can be heated to  $\sim 5000K$  and ionized by the radiation. The maximum disk luminosity of the true quiescent state occurs with the inner disk radius at the light cylinder,  $r_{lc} = c/\omega_s = r_m$ . The maximum luminosity of the quiescent state is typically a factor of a few larger than the average observed quiescent luminosity.

$$L_{q,max} = (2.7 \times 10^{30} \text{ erg/s}) \mu_{27}^2 \nu_2^{9/2} m^{1/2} \quad (43)$$

---

<sup>9</sup>The time for a luminosity variation to be observed is very long for energy released by processes inside the photon sphere.

We calculate the average quiescent luminosities in the soft x-ray band from  $\sim 0.5 - 10$  keV using the correlations of Possenti et al. [2002] with spin-down energy loss rate as:

$$L_q = \beta \dot{E} = \beta 4\pi^2 I \nu \dot{\nu} \quad (44)$$

where  $I$  is the moment of inertia of the star,  $\nu$  its rate of spin and  $\beta$  a multiplier that can be determined from this new  $\dot{E} - L_q$  correlation for given  $\dot{E}$ ; i.e., known spin and magnetic moment. In previous work we had used  $\beta = 10^{-3}$  for all objects, but  $\beta \sim 3 \times 10^{-4}$  would be the average value for GBHC-MECO consistent with the Possenti correlation. We assume that the luminosity is that of a spinning magnetic dipole for which  $\dot{E} = 32\pi^4 \mu^2 \nu^4 / 3c^3$ , (Bhattacharya & Srinivasan 1995) where  $\mu$  is the magnetic moment. Thus the quiescent x-ray luminosity would then be given by:

$$L_q = \beta \times \frac{32\pi^4 \mu^2 \nu^4}{3c^3} = 3.8 \times 10^{33} \beta \mu_{27}^2 \nu_2^4 \quad \text{erg/s} \quad (45)$$

According to the Possenti correlation,  $\beta = L_q / \dot{E} \propto \dot{E}^{0.31}$ .  $\beta$  should be a dimensionless, ratio, and independent of mass. But since  $\dot{E}$  is proportional to mass, we extend the Possenti relation, without loss of generality, to provide a mass scale invariant quantity. We therefore take  $\beta \propto (\dot{E}/m)^{0.31}$ . From the Possenti correlation, assuming all the objects in their study have the canonical  $m = 1.4$ , we then find that

$$\beta = 7 \times 10^{-4} (\dot{E}/m)^{0.31} = 4.6 \times 10^{-4} (10^{-36} L_c \nu_2)^{0.31} \quad (46)$$

Since the magnetic moment,  $\mu_{27}$ , enters each of the above luminosity equations it can be eliminated from ratios of these luminosities, leaving relations involving only masses and spins. For known masses, the ratios then yield the spins. Alternatively, if the spin is known from burst oscillations, pulses or spectral fit determinations of  $r_c$ , one only needs one measured luminosity,  $L_c$  or  $L_{min}$  at the end of the transition into the soft state, to enable calculation of the remaining  $\mu_{27}$  and  $L_q$ . For some GBHC, we found it to be necessary to estimate the co-rotation radius from multicolor disk fits to the thermal component of low state spectra. The reason for this is that the luminosities are sometimes unavailable across the whole spectral hardening transition from  $L_c$  to  $L_{min}$  for GBHC.

For GBHC, it is a common finding that the low state inner disk radius is much larger than that of the marginally stable orbit; e.g. [Markoff, Falcke & Fender 2001, Życki, Done & Smith 1997a,b 1998, Done & Życki 1999, Wilson & Done 2001]. The presence of a magnetosphere is an obvious explanation. Given an inner disk radius at the spectral state transition, the GBHC spin frequency follows from the Kepler relation  $2\pi\nu_s = \sqrt{GM/r^3}$ .

Although we have taken our model and used it to predict the spin rates and accurate quiescent luminosities for NS and GBHC that are shown in Table 1, it now appears that we could use the fact that the model fits well to calculate more accurate parameters. By placing the last mass scale invariant Possenti relation for

$\beta$  into the relation for quiescent luminosity and using it with the expression for  $L_c$ , we can determine spin rates to be given by

$$\nu = 89(L_{q,32}/(mL_{c,36}^{1.31}))^{1/1.31} \text{ Hz} \quad (47)$$

where  $L_{q,32} = 10^{-32}L_q$  and  $L_{c,36} = 10^{-36}L_c$ . Using this relation and the equation for  $L_c$ , the average spin rate for the GBHC of Table 1 is reduced to 10 Hz and the average GBHC magnetic moment is found to be 2200 gauss-cm<sup>3</sup>. These results essentially preserve the quiescent luminosities and actually should be more reliably determined because luminosity measurements are more reliable than inner disk radii determined from spectral fitting.<sup>10</sup>

## 9 Low State Mass Ejection and Radio Emission

The radio flux,  $F_\nu$ , of jet sources has a power law dependence on frequency of the form

$$F_\nu \propto \nu^{-\alpha} \quad (48)$$

It is believed to originate in jet outflows and has been shown to be correlated with the low state x-ray luminosity [Merloni, Heinz & DiMatteo 2003], with  $F_\nu \sim L_x^{0.7}$ . The radio luminosity of a jet is a function of the rate at which the magnetosphere can do work on the inner ring of the disk. This depends on the relative speed between the magnetosphere and the inner disk; i.e.,  $\dot{E} = \tau(\omega_s - \omega_k)$ , or

$$\dot{E} = \left(\frac{\lambda\delta r}{r}\right) \frac{\mu^2\omega_s(1 - \frac{\omega_k}{\omega_s})}{r^3} \propto \mu^2 M^{-3} \dot{m}_{Edd}^{6/7} \omega_s \left(1 - \frac{\omega_k}{\omega_s}\right) \quad (49)$$

Here  $\dot{m}_{Edd}$  is the mass accretion rate divided by the rate that would produce luminosity at the Eddington limit for mass  $M$ .

Disk mass, spiraling in quasi-Keplerian orbits from negligible speed at radial infinity must regain at least as much energy as was radiated away in order to escape. For this to be provided by the magnetosphere requires  $\dot{E} \geq GM\dot{M}/2r$ , from which  $\omega_k \leq 2\omega_s/3$ . Thus the magnetosphere alone is incapable of completely ejecting all of the accreting matter once the inner disk reaches this limit and the radio luminosity will be commensurately reduced and ultimately cut off at maximum x-ray luminosity for the low state and  $\omega_k = \omega_s$ . Typical data for GX339-4 [Gallo, Fender & Pooley 2003] are shown in Figure 1. For very rapid inner disk transit through the corotation radius, fast relative motion between inner disk and magnetosphere can heat the inner disk plasma and strong bursts of radiation pressure from the central object may help to drive large outflows while an extended jet structure is still largely intact. This process has been calculated<sup>11</sup> using pressures and poloidal magnetic

<sup>10</sup>MECO Magnetic moments must scale as  $m^{5/2}$ . Then for consistent change of results reported in Table 1, this requires  $L_{c,36}/(m^4\nu^3) = 1$ .

<sup>11</sup>though for inner disk radii inside the marginally stable orbit [Chou & Tajima 1999]

fields of unspecified origins. A MECO is obviously capable of supplying both the field and a radiation pressure. The hysteresis of the low/high and high/low state transitions may be associated with the need for the inner disk to be completely beyond the corotation radius before a jet can be regenerated after it has subsided.

Since  $\dot{E} \propto r^{-3}$  and  $L_d \propto r^{-9/2}$ , it is apparent that we should expect radio luminosity,  $L_R \propto L_d^{2/3}$ . In particular we find

$$L_R = C(M, \beta, \omega_s) 2L_c^{1/3} L_d^{2/3} (1 - \omega_k/\omega_s) \quad (50)$$

where  $\beta = \mu/M^3$  and  $C(M, \beta, \omega_s)$  is a constant, dependent on the radio bandpass. It has been analyzed and evaluated [Robertson & Leiter 2004]. The cutoff at  $\omega_k = \omega_s$  is shown by the line on Figure 1. The cutoff typically occurs with x-ray luminosity of  $\sim 0.01 - 0.02$  times Eddington luminosity. If we let  $x = L_d/L_c$ , then for  $x < 1$ , corresponding to the low state, Eq. (50) takes the form:

$$L_R = C(M, \beta, \omega_s) 2L_c(x^{2/3} - x) \quad (51)$$

The function has a maximum value of  $0.3C(M, \beta, \omega_s)L_c$  at  $x = 0.3$ .

Strictly speaking,  $L_d$ , in Eq. (50) should be the bolometric luminosity of the disk, however, the x-ray luminosity over a large energy band is a very substantial fraction of the disk luminosity. To compare with the correlation exponent of  $2/3$  obtained here, recent studies, including noisy data for both GBHC and AGN have yielded  $0.71 \pm 0.01$  [Gallo, Fender & Pooley 2003],  $0.72$  [Markoff et al. 2003, Falcke, K rding & Markoff 2003],  $0.60 \pm 0.11$  [Merloni, Heinz & Di Matteo 2003] and  $0.64 \pm 0.09$  [Maccarone, Gallo & Fender 2003]. For  $\alpha$  in the range (0 to -0.5),  $\beta \propto M^{-1/2}$ ,  $\omega_s \propto M^{-1}$  and  $L_c \propto M$ , the MECO model yields  $C(M) \propto M^{(9-4\alpha)/12}$  and (neglecting the cutoff region)

$$\log L_R = (2/3)\log L_x + (0.75 - 0.92)\log M + const. \quad (52)$$

which is a better fit to the ‘‘fundamental plane’’ of Merloni, Heinz & Di Matteo [2003] than any of the ADAF, disk/corona or disk/jet models they considered (see their Figure 5 for a  $\chi^2$  density plot). This last relation correctly describes the correlation for both GBHC and AGN.

## 10 Spectral States

The progression of configurations of accretion disk, magnetic field and boundary layer is shown for GBHC in Figure 2. The caption summarizes the spectral features expected in four regimes:

### Quiescence

In true quiescence, the inner disk radius is outside the light cylinder. In fact, it is usually far beyond the light cylinder, as the inner disk is ablated by  $\sim 10^{30-33}$

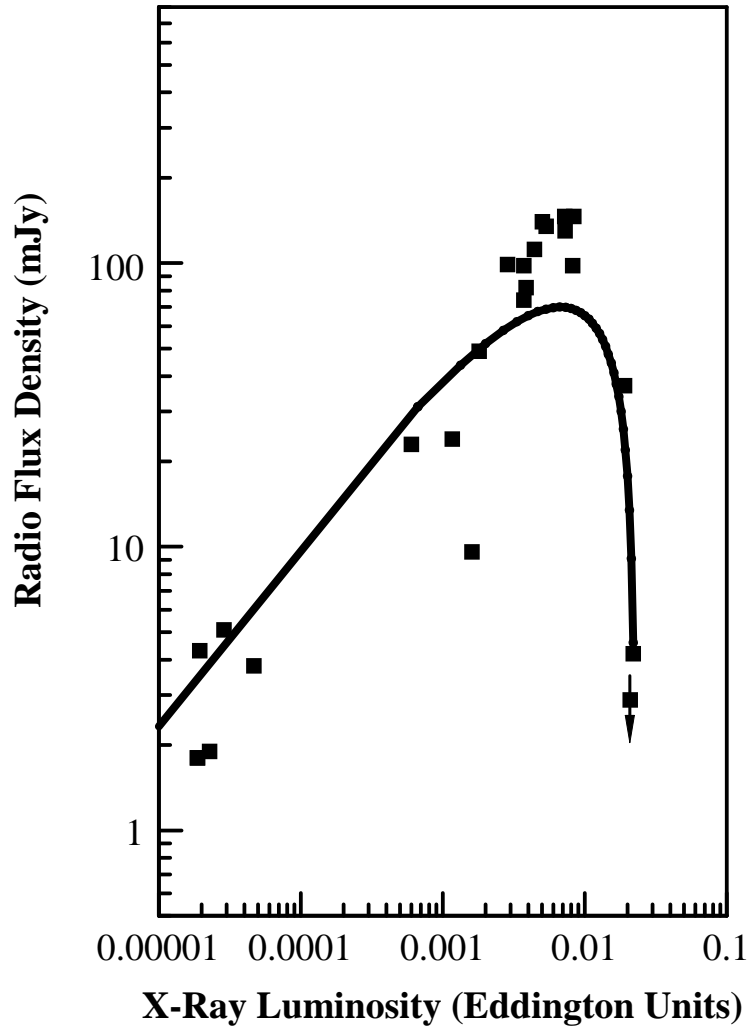


Figure 1: Radio/X-ray correlation for GX 339-4. Data from [Gallo, Fender & Pooley 2003]. The line is from Eq. (51) with  $L_c$  from Table 1, and  $C(M, \beta, \omega_s)$  crudely estimated. The line illustrates the predicted radio cutoff of the MECO model.

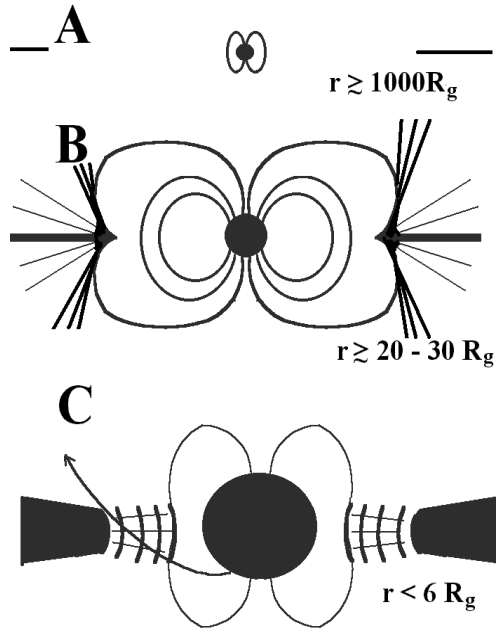


Figure 2: MECO Spectral States: **A quiescent:** Inner disk ablated, low accretion rate to inner ablation radius  $\sim 10^9 - 10^{10} cm$  generates optical emissions. Magnetic spin-down drives hard power-law x-ray spectrum. For NS, surface x-ray emissions may be visible. **B. Low state:** Thin, gas pressure dominated inner disk has large magnetically dominated viscosity. The inner disk radius lies between the light cylinder and co-rotation radii. Disk winds and jets are driven by the magnetic propeller. A hard spectrum is produced as most soft x-ray photons from the disk are Comptonized by either outflow or corona. Outflows of electrons on open magnetic field lines, possibly in jets, produce synchrotron radiation. Most of the outer disk is shielded from the magnetic field of the central object as surface currents in the inner disk change the topology of the magnetopause. **C: Intermediate and High state:** Once the inner disk is inside the co-rotation radius, the outflow and synchrotron emissions subside, but a steep power law spectrum is produced until the jet structure dies and an optically thick disk builds in to the marginally stable orbit. Relaxation oscillations may occur if radiation from the central object momentarily drives the inner disk back outside the co-rotation radius. A boundary layer of material beginning to co-rotate with the magnetosphere may push the magnetopause to the star surface for NS or inside  $r_{ms}$  for MECO, where a supersonic flow plunges inward until radiation pressure stabilizes the magnetopause or plasma interchange instabilities break up the flow. The MECO photosphere radiates a bright ‘ultrasoft’ thermal component. Bulk comptonization of many photons on spiral trajectories crossing the plunging zone inside  $r_{ms}$  produces a hard x-ray spectral tail. Declining phase hysteresis occurs since the soft luminosity can persist until the jet structure is rebuilt.

erg/s radiation from the central object. This luminosity is sufficient to raise the temperature of the optically thick inner disk above the  $\sim 5000$  K instability temperature for hydrogen out to a distance of  $r \sim 10^{10}$  cm. Therefore we expect the quiescent inner disk to be essentially empty. The rate of mass flow from ablation at the inner disk radius would only need to be  $\sim 10^{13}$  g/s to produce the quiescent optical emission observed for GBHC and NS. The ablated material could escape if it reached the magnetic propeller region, which is confined to the light cylinder at a much smaller radius,  $r_{lc}$ , than that of the inner disk. The ejection of the ablated material probably also produces the quiescent state power law x-ray spectrum. It likely would also produce weak radio emissions, but in this case the exponent of the radio/x-ray luminosity correlation would change from 2/3 to 1 as both would originate as optically thin synchrotron emissions.

The empty inner disk makes the MECO model compatible with the disk instability model of x-ray nova outbursts, which begin as ‘outside-in’ events in which substantial outer mass reservoirs have been observed to fill an accretion disk on the viscous timescale of a very subsonic radial flow [Orosz et al. 1997]. From true quiescence to the light cylinder, the x-ray luminosity changes by a factor of only a few. The accretion rate at  $L_{q,max}$  is only  $\dot{m} = 1.7 \times 10^{12} \mu_{27} \nu_2^{7/2} m^{-1/2} \sim 2 \times 10^{14}$  g/s.

Quiescent luminosities that are generally 10 - 100 X lower for GBHC than for NS have been claimed as evidence for the existence of event horizons. [Narayan et al. 1997, Garcia et al. 2001]. In the MECO model, the quiescent luminosity is driven by the magnetic dipole radiation from the spinning central magnetic moment. The lower quiescent luminosities of the GBHC are explained by their lower spin rates and (perhaps unobservably) low rates of quiescent emission from the central MECO.

### Low/Hard State

In the low state, the inner disk radius is inside the light cylinder, with hot, diamagnetic plasma reshaping the magnetopause topology [Arons et al. 1984]. This magnetic propeller regime (Ilarianov & Sunyaev 1975, Stella, White & Rosner 1986, Cui 1997, Zhang, Yu & Zhang 1997, Campana et al. 1998) exists until the inner disk pushes inside the co-rotation radius,  $r_c$ . From  $r_{lc}$  to  $r_c$ , the x-ray luminosity may increase by a factor of  $\sim 10^3 - 10^6$ . Inside  $r_c$ , large fractions of the accreting plasma can continue on to the central object and produce a spectral state switch to softer emissions. We have shown [Section 8 and Robertson & Leiter 2002] that magnetic moments and spin rates can be determined from luminosities at the end points of the transition from low/hard to high/soft spectral states. The magnetic moments and spins were used to calculate the  $\sim 10^{3-6}$  times fainter quiescent luminosities expected from spin-down. The results are recapitulated and extended in Table 1 and Appendix C. During waning phases of nova outbursts,  $L_c \sim 0.02 L_{Edd}$  can be identified as the maximum disk luminosity upon entering the low state.

Until the inner disk reaches  $r_c$ , accreting plasma is ejected. It may depart in a jet, or as an outflow back over the disk as plasma is accelerated on outwardly curved or open magnetic field lines. Radio images of both flows have been seen [Paragi et

al. 2002]. Equatorial outflows could contribute to the low state hard spectrum by bulk Comptonization of soft photons in the outflow, however, we think that the hard spectrum originates primarily in patchy coronal flares [Merloni & Fabian 2002] on a conventional geometrically thin, optically thick disk.<sup>12</sup> Both outflow comptonization and coronal flares are compatible with partial covering models for dipping sources, in which the hard spectral region seems to be extended [Church 2001, Church & Balucinska-Church 2001]. Alternatively, a compact jet [Corbel & Fender 2002] might be a major contributor to the hard spectrum, but if so, the x-ray luminosity must fortuitously match the power that would be dissipated in a conventional thin disk. Finally, we note that the power law emissions of the low/hard state are usually cut off below  $\sim 100$  keV, consistent with a coronal temperature of 20 – 50 keV. Bulk comptonization would be expected to produce higher energies.

### Intermediate (Steep Power-Law) State

Intermediate states typically occur with luminosities in the range  $(0.01 - 0.3)L_{Edd}$  when some, but not all, of the accreting matter can make its way to the central object. These states are usually observed with rising luminosity and often do not appear during declining phases. They are characterized by increasing luminosity, an increasing power law index and the presence of a weak, soft thermal contribution to the x-ray spectrum. The soft emissions originate, at least in part from the central object surface. The steep power law, extending well beyond 100 keV, is produced via bulk comptonization as soft photons scatter from the (initially) optically thin material entering the magnetosphere. Incomplete spectral state switches terminating well below the Eddington limit, such as those exhibited by Cygnus X-1 may occur. With the inner disk radius large ( $> 20R_g$ ) near co-rotation, there is a very large difference in the efficiency of energy release at the central object vs. the disk. Thus changes of luminosity and an apparent, but incomplete, spectral state switch can occur for very small change of accretion rate. Relaxation oscillations between hard and soft states, driven by intermittent radiation from the central object, can occur if the accretion rate is not steady. Large periodic jet ejections may be associated with this state, for which significant toroidal winding of the poloidal magnetic field lines and radiation pressure may contribute to the ejection. The intermediate state terminates in the high/soft state with the disk becoming optically thick all the way into the marginally stable orbit or a NS surface. This occurs at  $\sim (0.2 - 0.4)L_{Edd}$ . The outflow/jet of the low state is a substantial flow structure that is systematically disrupted as flow in the inner disk increases in the intermediate state.

### High/Soft (Thermally Dominant) State

With the disk inner radius inside  $r_c$ , the propeller regime ends and matter of sufficient pressure can make its way inward. With inner disk inside  $r_c$ , the outflow and/or jets subside, the system becomes radio quiet, and a soft thermal excess from the central object appears, [e.g., see Fig. 3.3 of Tanaka & Lewin, p. 140], which

---

<sup>12</sup>See the disk characteristics section below. Optically thick material is needed to produce pressures capable of countering magnetic pressure on the inner disk.

may be even be described as ‘ultrasoft’ [White & Marshall 1984]; particularly when the central object cools as the luminosity finally begins to decline<sup>13</sup>. We have shown that GBHC-MECO would produce a dominant ‘ultrasoft’ component at  $\sim 1.1$  keV in the high state. They would also continue to produce a steep power-law hard tail as soft photons leaving the MECO well inside the photon orbit take trajectories that take them across the plunging region inside the marginally stable orbit. Since there is no comparably rich source of photons on disk crossing trajectories for NS and a much smaller, if any, plunging region, there is no comparable hard spectral component produced by bulk comptonization in their high states.

In producing the the high/soft (thermally dominant) state the jet structure of the low/hard state is destroyed and an optically thick disk progressively pushes inside  $r_c$ , shredding the magnetic field lines as it encroaches. The flow into the magnetosphere is initially optically thin, but eventually gives way to an optically thick disk that reaches the marginally stable orbit (or star surface in NS systems). The steep power law spectrum becomes increasingly dominant and then its luminosity may decline (while photon energies increase) as the optically thick part of the disk encroaches. After the soft state has peaked and begun to decline, the flow remains organized as a disk flow until the magnetosphere can expand beyond  $r_c$ , eject inner disk material and rebuild the magnetic tower structure of a jet. At this point the luminosity is  $L_c \sim 0.02L_{Edd}$ . The transition into the high/soft state occurs at  $\sim (0.2 - 0.4)L_{Edd}$ , hence there is a hysteresis of the hard  $\rightarrow$  soft transition compared to the soft  $\rightarrow$  hard transition.

## 11 Disk Characteristics

For matter sufficiently inside  $r_c$ , the propeller mechanism is incapable of stopping the flow, however, a boundary layer may form at the inner disk radius in this case. The need for a boundary layer for GBHC can be seen by comparing the magnetic pressure at the magnetosphere with the impact pressure of a trailing, subsonic disk. For example, for an average GBHC magnetic moment of  $\sim 4 \times 10^{30}$  gauss cm<sup>3</sup> (see the last of Section 8), the magnetic pressure at a  $r_{ms}$  radius of  $6.3 \times 10^6$  cm for a  $7 M_\odot$  GBHC would be  $B^2/8\pi \sim 10^{19}$  erg/cm<sup>3</sup>. At a mass flow rate of  $\dot{m} = 10^{18}$  g/s, which would be near Eddington limit conditions for a  $7 M_\odot$  MECO, the inner disk temperature would be  $T \sim 1.5 \times 10^7$  K. A thin disk scale height, well behind its inner edge, would be given by  $H \sim rv_s/v_K \sim 0.0036r$ , where  $v_s \sim 4.5 \times 10^7$  cm/s and  $v_K \sim 1.2 \times 10^{10}$  cm/s are acoustic and Keplerian speeds, respectively. The impact pressure would be  $\dot{m}v_r/4\pi rH \sim 5.6 \times 10^5 v_r$  erg/cm<sup>3</sup>. It would require  $v_r$  in excess of the speed of light to let the impact pressure match the magnetic pressure. But since the magnetic field doesn’t eject the disk material inside  $r_c$ , matter piles up as essentially dead weight against the magnetopause and pushes it in. The radial extent of such a layer would only need to be  $\sim kT/m_p g \sim 50$  cm, where  $m_p$  is the proton

<sup>13</sup>Due to the high redshift, the MECO luminosity decay can be very slow.

mass and  $g$ , the radial gravitational free fall acceleration, but it is likely distributed over a larger transition zone from co-rotation with the magnetosphere to Keplerian flow. The gas pressure at the inner radius of the transition zone necessarily matches the magnetic pressure. In this case, radiation pressure in the disk, at  $T = 1.5 \times 10^7 K$ , is nearly three orders of magnitude below the gas pressure. Therefore a gas pressure dominated, thin, Keplerian disk with subsonic radial speed should continue all the way to  $r_{ms}$  for a MECO. Merloni & Fabian [2002] have shown that an accretion disk corona can account for the hard spectrum of the low state for a gas pressure dominated disk. Similar conditions occur with disk radius inside  $r_c$  even for weakly magnetic ‘atoll’ class NS. The similar magnetic pressures at  $r_c$  for GBHC and atolls is one of the reasons for their spectral and timing similarities.

In the case of NS, sufficiently high mass accretion rates can push the magnetopause into the star surface, but this requires near Eddington limit conditions. At this point the hard apex of the right side of the horizontal branch of the ‘Z’ track in the hardness/luminosity diagram is reached. It has recently been shown [Muno et al. 2002] that the distinction between ‘atoll’ and ‘Z’ sources is merely that this point is reached near the Eddington limit for ‘Zs’ and at perhaps  $\sim 10 - 20\%$  of this luminosity [Barrett & Olive 2002] for the less strongly magnetized ‘atolls’. Atolls rarely reach such luminosities. For MECO based GBHC, one would expect a relatively constant ratio of hard and soft x-ray ‘colors’ after the inner disk crosses  $r_c$  and the flow reaches the photon orbit. If x-ray ‘color’ bands for GBHC were chosen below and above a  $\sim 1keV$  thermal peak similarly to way they are now chosen to bracket the  $\sim 2keV$  peak of NS, one might observe a ‘Z’ track for the color/color diagrams of GBHC.

An observer at coordinate,  $r$ , inside  $r_{ms}$ , would find the radial infall speed to be  $v_r = \frac{\sqrt{2}}{4}c(6R_g/r-1)^{3/2}$ , (see Appendix A) and the Lorentz factor for a particle spiraling in from  $6R_g$  would be  $\gamma = 4\sqrt{2}(1+z)/3$ , where  $1+z = (1-2R_g/r)^{-1/2}$  would be the red shift for photons generated at  $r$ . If the distantly observed mass accretion rate would be  $\dot{m}_\infty$ , then the impact pressure at  $r$  would be  $p_i = (1+z)\dot{m}_\infty\gamma v_r/(4\pi rH)$ . For  $\dot{m}_\infty \sim 10^{18}$  g/s, corresponding to Eddington limit conditions for a  $7 M_\odot$  GBHC, and  $H = 0.0036r$ , impact pressure is,  $p_i \sim 5 \times 10^{16}(1+z)^2(2R_g/r)^2(6R_g/r-1)^{3/2}$  erg/cm<sup>3</sup>. For comparison, the magnetic pressure is  $(1+z)^2 B_\infty^2/8\pi$ . Assuming a dipole field with average magnetic moment of  $4 \times 10^{30}$  gauss cm<sup>3</sup> (see Section 8), the magnetic pressure is  $\sim 10^{22}(1+z)^2(2R_g/r)^6$  erg/cm<sup>3</sup>. Thus there are no circumstances for which the impact pressure is as large as the magnetic pressure for  $2R_g < r < 6R_g$ . We conclude that another weighty boundary layer must form inside  $r_{ms}$  if the magnetosphere is to be pushed inward. More likely, the plasma stream is broken up by Kelvin-Helmholtz instabilities and filters through the magnetosphere. In any event, the inner radius of the disk is determined by the rate at which the magnetic field can strip matter and angular momentum from the disk. This occurs in a boundary layer of some thickness,  $\delta r$ , that is only a few times the disk thickness.

Other than the presence of a transition boundary layer on the magnetopause,

the nature of the flow and spectral formation inside  $r_c$  is a research topic. Both the short radial distance from  $r_c$  to  $r_{ms}$  and the magnetopause topology should help to maintain a disk-like flow to  $r_{ms}$ . Radial acceleration inside  $r_{ms}$  should also help to maintain a thin flow structure. These flows are depicted in Figure 2. Recapitulating, we expect the high state flow into the MECO to produce a distantly observed soft thermal component, part of which is strongly bulk Comptonized.

### Quasi-periodic Oscillations

Although many mechanisms have been proposed for the high frequency quasi-periodic oscillations (QPO) of x-ray luminosity, they often require conditions that are incompatible with thin, viscous Keplerian disks. Several models have requirements for lumpy flows, elliptical inner disk boundaries, orbits out of the disk plane or conditions that should produce little radiated power. In a conventional thin disk, the vertical oscillation frequency, which is approximately the same as the Keplerian frequency of the inner viscous disk radius should generate ample power. Accreting plasma should periodically wind the poloidal MECO magnetic field into toroidal configurations until the field lines break and reconnect across the disk. Field reconnection across the disk should produce high frequency oscillations that couple to the vertical oscillations. If so, there would be an automatic association of high frequency QPO with the harder power-law spectra of magnetospherically driven emissions, as is observed. Mass ejection in low state jets might be related to the heating of plasma via the field breakage mechanism, in addition to natural buoyancy of a plasma magnetic torus in a poloidal external field.

It seems possible that toroidal winding and reconnection of field lines at the magnetopause, might continue in high states inside  $r_{ms}$ . If so, there might be QPO that could be identified as signatures of the MECO magnetosphere. If they occur deep within the magnetosphere, they might be at locally very high frequencies, and be observed distantly as very redshifted low frequencies. As shown in Appendix A, the spiral orbit infall frequencies in the plunging region inside  $r_{ms}$  are given by  $\nu = 1.18 \times 10^5 (R_g/r)^2 (1 - 2R_g/r)/m$  Hz. A maximum frequency of 437 Hz would occur for  $m=10$  at the photon orbit. Of more interest, however are frequencies for  $R_g/r \approx 1/2$ , for which  $\nu = 2950/(m(1+z)^2)$  Hz. For  $1+z = 10 - 100, m = 10$ ; conditions that might apply to the photosphere region,  $\nu \sim 0.03 - 3$  Hz could be produced. In this regard, one could expect significant time lags between inner disk accretion and luminosity fluctuations and their echoes from the central highly redshifted MECO.

Even if QPO are not produced inside  $r_{ms}$  or inside the photon sphere for GBHC, there is an interesting scaling mismatch that might allow them to occur for AGN. Although the magnetic fields of AGN scale as  $m^{-1/2}$ , the velocity of plasma at and inside  $r_{ms}$  does not. Thus the energy density of disk plasma inside  $r_{ms}$  will be relatively larger than magnetic field energy densities for AGN accretion disks. When field energy density is larger than kinetic energy density of matter, the field pushes matter around. When the reverse is true, the matter drags the field along. Thus

toroidal winding of the field at the magnetopause could fail to occur for GBHC, but might easily occur in AGN. If the process is related to mass ejection, then very energetic jets with Lorentz factors  $\gamma \sim (1+z) > 10$  might arise from within  $r_{ms}$  for AGN. A field line breakage model of ‘smoke ring’ like mass ejection from deep within  $r_{ms}$  has been developed by Chou & Tajima [1999]. In their calculations, a pressure of unspecified origin was needed to stop the flow outside  $2R_g$  and a poloidal magnetic field, also of unspecified origin was required. MECO provide the necessary ingredients in the form of the intrinsic MECO magnetic field. The Chou & Tajima mechanism, aided by intense radiation pressure, may be active inside  $r_{ms}$  for GBHC and produce extremely large episodic mass ejections such as those shown by GRS 1915+105. Although not developed for conditions with large inner disk radius, the same magnetic reconnection mechanism probably produces the jet emissions [Goodson, Bohm & Winglee 1999] associated with the low/hard state [Gallo, Fender & Pooley 2003].

Finally, some of the rich oscillatory behavior of GRS 1915+105 may be readily explained by the interaction of the inner disk and the central MECO. The objects in Table 1 have co-rotation radii of order  $(20 - 50)R_g$ , which brings the low state inner disk radius in close to the central object. A low state MECO, balanced near co-rotation would need only a small increase of mass flow rate to permit mass to flow on to the central MECO. This would produce more than 20X additional luminosity and enough radiation pressure to blow the inner disk back beyond  $r_c$  and load its mass onto the magnetic field lines where it is ejected. This also explains the association of jet outflows with the oscillatory states. Belloni et al. [1997] have shown that after ejection of the inner disk of GRS 1915+105, it then refills on a viscous time scale until the process repeats. Thus one of the most enigmatic GBHC might be understood as a relaxation oscillator, for which the frequency is set by a critical mass accretion rate.

## 12 Detecting MECO

It may be possible to detect MECO in several ways. Firstly, as we have shown, for a red shift of  $z \sim 10^8$ , the quiescent luminosity of a GBHC MECO would be  $\sim 10^{31}$  erg/s with  $T_\infty \sim 0.01$  keV. This thermal peak might be observable for nearby GBHC, however it has not been found for the high galactic latitude GBHC, XTE J1118+480. Secondly, at moderate luminosities  $L \sim 10^{36} - 10^{37}$  erg/s but in a high state at least slightly above  $L_c$ , a central MECO would be a bright, small central object that might be sharply eclipsed in deep dipping sources. A high state MECO should stand out as a small bright source. This is consistent with analyses of absorption dips in GBHC GRO J1655-40 [Church 2001] which have shown the soft source of the high state to be smaller than the region that produces the hard spectral component of its low states. A conclusive demonstration that most of the soft x-ray luminosity of a high state GBHC is distributed over a large accretion disk

would be inconsistent with MECO or any other GBHC model entailing a central bright source. If the MECO model is correct, the usual identification of the bright, high state soft component as disk emissions is wrong. Fitting high state spectra to multicolor disk (MCD) blackbody models produces temperatures,  $T_\infty$ , that are consistent with MECO, but due to the normalization of MCD, the inner disk radii obtained are exactly  $\sqrt{3}$  times the radius of a MECO. The apparent constant MCD radii over a large range of high state luminosity may merely misrepresent a constant MECO radius that is  $\sqrt{3}$  times smaller. Thirdly, a pair plasma atmosphere in an equipartition magnetic field should be virtually transparent to photon polarizations perpendicular to the magnetic field lines. The x-rays from the central MECO should exhibit some polarization that might be detectable, though this is far from certain since the distantly observed emissions could originate from nearly any point on the photosphere and then appear to originate from the photon sphere. MECO presumably would not be found only in binary systems. If they are the offspring of massive star supernovae, then they should be found all over the galaxy. If we have correctly estimated their quiescent temperatures, isolated MECO-GBHC would be weak, possibly polarized, EUV sources with a power-law tail in soft x-rays. In subsequent work we may find additional signatures of MECO among the AGN.

### 13 Conclusion

It is now becoming apparent that many of the spectral properties of LMXB, including the GBHC, are consistent with the existence of intrinsically magnetized central objects. We have shown that the existence of intrinsically magnetic GBHC is consistent with a new class of magnetospheric eternally collapsing object (MECO) solutions of the Einstein field equations of General Relativity. These solutions are based on a strict adherence to the SPOE requirement for timelike world line completeness; i.e., that the world lines of physical matter under the influence of gravitational and non-gravitational forces must remain timelike in all regions of spacetime. Since there is nothing in the structure of the Einstein tensor,  $G^{\mu\nu}$ , on the left hand side of the Einstein field equation that dynamically enforces ‘time like world line completeness’, we have argued that the SPOE constrains the physically acceptable choices of the energy momentum tensor,  $T^{\mu\nu}$  to contain non-gravitational forces that can dynamically enforce it. In this context we have found the long-lived MECO solutions. As these are necessarily based on a radiating Vaidya metric, there is no transformation to the Kerr-Schild coordinates used in black hole models.

An enormous body of physics scholarship developed primarily over the last half century has been built on the assumption that trapped surfaces leading to event horizons and curvature singularities exist. Misner, Thorne & Wheeler [1973], for example in Sec. 34.6 clearly state that this is an assumption and that it underlies the well-known singularity theorems of Hawking and Penrose. In contrast, we have found that strict adherence to the SPOE demand for timelike world line completeness

requires a ‘*no trapped surface condition*’. This has led to the quasi-stable, high red shift MECO solutions of the Einstein field equations. The physical mechanism of their stable rate collapse is an Eddington balance maintained by the distributed photon generation of a highly compact and redshifted equipartition magnetic field. This field also serves to confine the pair plasma dominated outer layers of the MECO and the thin MECO pair atmosphere. Red shifts of  $z \sim 10^8(m/7)^{1/2}$  have been found to be necessary for compatibility with our previously found magnetic moments for GBHC.

In this chapter we have given detailed descriptions of MECO properties and shown that standard gas pressure dominated ‘alpha’ accretion disks would be compatible with them. We have shown that the magnetosphere/disk interaction affects nearly all of the spectral characteristics of NS and GBHC in LMXB systems and accounts for them in a unified and complete way, including jet formation and radio emissions. This model is solidly consistent with accreting NS systems, for which intrinsic magnetic moments obtained from spin-down measurements allow little choice. Even their relatively weak magnetic fields are too strong to ignore. Since the similar characteristics of GBHC are cleanly explained by the same model, the MECO offers a unified theory of LMXB phenomenology as well as extensions to AGN. Since MECO lifetimes are orders of magnitude greater than a Hubble time, they provide an elegant and unified framework for understanding the broad range of observations associated with GBHC and AGN. Lastly we have indicated some ways in which the existence of MECO in GBHC and AGN might be detected and confirmed.

## Appendix A. Relativistic Particle Mechanics

A number of standard, but useful results for relativistic mechanics are recapitulated here. All are based upon the energy-momentum four-vector for a free particle in the singularity-free Finkelstein or Kerr-Schild coordinates for a constant central mass. Though not strictly compatible with radiating objects with variable mass, outgoing Finkelstein coordinates are a useful first order approximation to the outgoing Vaidya coordinates for low radiation rates exterior to a MECO.

$$ds^2 = c^2 dt^2 ((1 - 2R_g/r) \pm 4R_g v^r / r - (1 + 2R_g/r) v^r v^r) - r^2 (d\theta^2 + \sin^2 \theta d\phi^2) \quad (53)$$

The plus sign corresponds to outgoing Finkelstein coordinates and the negative sign to ingoing Finkelstein or Kerr-Schild coordinates. Here  $v^r = dr/cdt$ . For a particle in an equatorial trajectory ( $\theta = \pi$ ,  $p_\theta = 0$ ) about an object of gravitational mass  $M$ , one obtains the same equation as for Schwarzschild coordinates:

$$\left(\frac{dr}{d\tau}\right) = -c(e^2 - (1 - 2R_g/r)(1 + a^2(R_g/r)^2))^{1/2} \quad (54)$$

Where  $e$  is the conserved energy per unit rest mass,  $a = (cp_\phi/GMm_0)$  is a dimensionless, conserved angular momentum,  $\tau$  is the proper time in the particle frame

and the negative sign indicates movement toward  $r = 0$ . The metric Eq. (53) also describes radial geodesics with  $ds^2 = d\tau^2$ . Neglecting angular terms and letting  $q = dt/d\tau$  and  $p = dr/d\tau$ , this equation can be written as

$$1 = (1 - 2R_g/r)q^2 \pm 4pqR_g/r - (1 + 2R_g/r)p^2 \quad (55)$$

With  $p$  given above, and  $a = 0$  this equation has the solution

$$q = \frac{+\sqrt{e^2} \pm 2R_g/r \sqrt{e^2 - (1 - 2R_g/r)}}{1 - 2R_g/r} \quad (56)$$

where the positive sign on the first radical has been taken to assure that time proceeds in a positive direction during the fall, and a positive second term again corresponds to outgoing coordinates. Since  $v^r = p/q$ , it is a straightforward matter to substitute for  $v^r$  in the original metric equation and examine the limit as  $R_g/r \rightarrow 1/2$ . In outgoing coordinates, we find that  $ds^2 \rightarrow 0$  as  $R_g/r \rightarrow 1/2$ .

It is of interest, however, that in the outgoing coordinates ( $+4R_g/r$ ) as  $R_g/r \rightarrow 1/2$  one finds  $v^r \rightarrow 0, q \rightarrow \infty, p \rightarrow -e$ . Thus it takes an infinite coordinate time, but only a finite proper time to cross the horizon, which is the same as the well-known Schwarzschild result. In the ingoing coordinates, one obtains  $v^r \rightarrow 0, q \rightarrow e, p \rightarrow -e$ . In either case, it is interesting to observe that the physical three-speed approaches that of light at the horizon [Landau & Lifshitz 1975].

$$V^2 = \left(\frac{dl}{d\tau_s}\right)^2 = c^2 \frac{(g_{0r}g_{0r} - g_{rr}g_{00})v^r v^r}{(g_{00} + g_{0r}v^r)^2} \quad (57)$$

Here we find  $V \rightarrow c$  as  $g_{00} \rightarrow 0$ . Finally, it should be mentioned that the vanishing of  $g_{00}$  for  $r > 0$  is actually a result of a failure to apply appropriate boundary conditions for the solutions of the Einstein equations for a point mass [Abrams 1979, 1989].

For suitably small energy, bound orbits occur. Turning points for which  $dr/d\tau = 0$  can be found by examining the effective potential, which consists of all terms to the right of  $e^2$  in Eq. (54). At minima of the effective potential we find circular orbits for which

$$a^2 = \frac{1}{R_g/r - 3(R_g/r)^2} \quad (58)$$

$R_g/r = 1/3$  holds at the location of an unstable circular orbit for photons (see below). From which we see that if  $p_\phi$  is non-zero there are no trajectories for particles with both mass and angular momentum that exit from within  $R_g/r = 1/3$ . Thus particles with both mass and angular momentum can't escape from within the photon sphere. The minimum energy required for a circular orbit would be.

$$E = m_0 c^2 \frac{(1 - 2R_g/r)}{\sqrt{(1 - 3R_g/r)}} \quad (59)$$

In fact, however, there is an innermost marginally stable orbit for which the first two derivatives with respect to  $1/r$  of the effective potential vanish. This has no Newtonian physics counterpart, and yields the well-known results:  $R_g/r = 1/6$ ,  $a^2 = 12$  and  $e^2 = 8/9$  for the marginally stable orbit of radius  $r_{ms} = 6GM/c^2$ .

For a particle beginning a spiral descent from  $r_{ms}$  with  $e = \sqrt{8/9}$ , there follows:

$$\left(\frac{dr}{d\tau}\right)^2 = c^2 \frac{(6R_g/r - 1)^3}{9} \quad (60)$$

If observed by a stationary observer located at coordinate  $r$ , it would be observed to move with radial speed

$$V_r = \frac{\sqrt{2}c(6R_g/r - 1)^{3/2}}{4}. \quad (61)$$

Again,  $V_r$  approaches  $c$  as  $R_g/r$  approaches  $1/2$ . A distant observer would find the angular frequency of the spiral motion to be

$$\begin{aligned} \frac{1}{2\pi} \frac{d\phi}{dt} &= \sqrt{9 \times 12/8} (c^3/GM) (R_g/r)^2 (1 - 2R_g/r) / 2\pi \\ &\sim 1.18 \times 10^5 (R_g/r)^2 (1 - 2R_g/r) / m \quad \text{Hz} \end{aligned} \quad (62)$$

For a  $10 M_\odot$  GBHC ( $m = 10$ ), this has a maximum of 437 Hz and some interesting possibilities for generating many QPO frequencies, both high and low. For red shifts such that  $R_g/r \approx 1/2$ , the spiral frequency is  $2950/(1+z)^2$  Hz.

### Photon Trajectories:

The energy-momentum equation for a particle with  $m_0 = 0$  can be rearranged as:

$$(1 - 2R_g/r)^2 \left(\frac{p_r GM}{p_\phi c^2}\right)^2 = \left(\frac{d(R_g/r)}{d\phi}\right)^2 = \left(\frac{GME}{p_\phi c^3}\right)^2 - (R_g/r)^2 (1 - 2R_g/r) \quad (63)$$

The right member has a maximum value of  $1/27$  for  $R_g/r = 1/3$ . There is an unstable orbit with  $d(R_g/r)/d\phi = 0$  for  $R_g/r = 1/3$ . To simply have  $d(R_g/r)/d\phi$  be real requires  $p_\phi c^3/GME < \sqrt{27}$ . But  $E = (1+z)pc$ , where  $p$  is the entire momentum of the photon, and  $1+z = (1 - 2R_g/r)^{-1/2}$  its red shift if it escapes to be observed at a large distance. Its azimuthal momentum component will be  $p_\phi/r$ . Thus its escape cone is defined by:

$$\left(\frac{p_\phi}{rp}\right)^2 < 27(R_g/r)^2 (1 - 2R_g/r) \quad (64)$$

For  $r_s \approx 2R_g$ , this approaches  $27/(4(1+z_s)^2)$ .

## Appendix B. Pair Plasma Photosphere Conditions

The photosphere condition is that [Kippenhahn & Weigert 1990]:

$$n_{\pm}\sigma_T l = 2/3, \quad (65)$$

where  $n_{\pm}$  is the combined number density of electrons and positrons in equilibrium with a photon gas at temperature  $T$ ,  $\sigma_T = 6.65 \times 10^{-25} \text{cm}^2$  is the Thompson scattering cross section and  $l$  is a proper length over which the pair plasma makes the transition from opaque to transparent. Landau & Lifshitz [1958] show that

$$n_{\pm} = \frac{8\pi}{h^3} \int_0^{\infty} \frac{p^2 dp}{\exp(E/kT) + 1} \quad (66)$$

where  $p$  is the momentum of a particle,  $E = \sqrt{p^2 c^2 + m_e^2 c^4}$ ,  $k$  is Boltzmann's constant,  $h$  is Planck's constant and  $m_e$ , the mass of an electron. For low temperatures such that  $kT < m_e c^2$  this becomes:

$$n_{\pm} \approx 2 \left( \frac{2\pi m_e kT}{h^2} \right)^{3/2} \exp(-m_e c^2 / kT) = 2.25 \times 10^{30} (T_9/6)^{3/2} \exp(-6/T_9) / \text{cm}^3 \quad (67)$$

where  $T_9 = T/10^9 \text{K}$ .

For a photosphere temperature of  $4 \times 10^8 \text{K}$ , for  $m = 7$ , the number density of pairs is  $n_{\pm} = 1.4 \times 10^{22} / \text{cm}^3$ , with the proper density reduced from this value by  $1 + z_p$ . The mean free path of photons among these is  $\sim 100 \text{cm}$  for a Thompson scattering cross-section of  $6.65 \times 10^{-25} \text{cm}^2$ . Considering the extreme redshift variation over a small radial coordinate interval, (Eq. (27)), the proper interval corresponding to a mean free path of  $\sim 100 \text{cm}$  would be expanded by a redshift factor somewhere between  $1 + z_p$  and  $(1 + z_s)$  to the range  $10^{5,10} \text{cm}$ ; i.e, to a normal and reasonable photosphere depth. To a distant observer, the pair atmosphere would occur in an extremely small coordinate interval. Modeling it numerically would be very difficult. As previously noted. the photosphere temperature is very nearly independent of the mass of the MECO.

At a surface temperature of  $6 \times 10^9 \text{K}$ , we find a proper pair density of  $n_{\pm} \sim 2.25 \times 10^{30} / (1 + z_s) / \text{cm}^3$ , which produces a maximum possible pair pressure  $\sim n_{\pm} m_e c^2 / 3$  some  $10^9$  times less than the radiation pressure. This justifies our use of radiation dominated pressure in the pair atmosphere. As shown in Appendix D, we expect  $n_{\pm} \sim 10^{22} / \text{cm}^3$  from consideration of the surface magnetic fields. For a  $m = 10$  MECO, this is just about what we get for  $T = 6 \times 10^9 \text{K}$ .

## Appendix C. New Observations

The third accreting millisecond pulsar, **XTE J0929-314** has been found [Galloway et al. 2002] with  $\nu_s = 1/P = 185 \text{Hz}$  and period derivative  $\dot{P} = 2.69 \times 10^{-18}$ ,

from which the magnetic field (calculated as  $3.2 \times \sqrt{P\dot{P}}$ ) is  $3.9 \times 10^9$  gauss. This is typical of a Z source. Assuming a NS radius of 13 km, the magnetic moment is  $BR^3 = 8.5 \times 10^{27}$  gauss cm<sup>3</sup>. The calculated low state limit co-rotation luminosity is  $L_c = 4.9 \times 10^{36}$  erg/s. Approximately 40% of this would be the luminosity in the (2 - 10 keV) band. This yields an expected flux of  $2 \times 10^{-10}$  erg/cm<sup>2</sup>/s for a distance of 9 kpc. This corresponds to the knee of the published light curve where the luminosity begins a rapid decline as the propeller becomes active. Similar breaking behavior has been seen in Sax J1808.4-3659 and GRO J1655-40 at propeller onset. The predicted 0.5-10 keV band luminosity is  $L_q = 1.3 \times 10^{33}$  erg/s.

The second accreting millisecond pulsar **XTE J1751-305** was found with a spin of 435 Hz. [Markwardt et al. 2002] Its spectrum has been analyzed [Miller et al. 2003]. We find a hard state luminosity of  $3.5 \times 10^{36}$  erg/s ( $d = 8$  kpc) at the start of the rapid decline which is characteristic of the onset of the propeller effect. We take this as an estimate of  $L_c$ . From this we estimate a magnetic moment of  $1.9 \times 10^{27}$  gauss cm<sup>3</sup> and a quiescent luminosity of  $5 \times 10^{33}$  erg/s. An upper limit on quiescent luminosity of  $1.8 \times 10^{34}$  erg/s can be set by the detections of the source in late April 2002, as reported by Markwardt et al. [2002].

The accreting x-ray pulsar, **GRO J1744-28** has long been cited for exhibiting a propeller effect. Cui [1997] has given its spin frequency as 2.14 Hz and a low state limit luminosity as  $L_c = 1.8 \times 10^{37}$  erg/s (2 - 60 keV.), for a distance of 8 kpc. These imply a magnetic moment of  $1.3 \times 10^{31}$  gauss cm<sup>3</sup> and a magnetic field of  $B = 5.9 \times 10^{12}$  gauss for a 13 km radius. Its spin-down energy loss rate should be  $\dot{E} = 1.4 \times 10^{35}$  erg/s and its quiescent luminosity,  $L_q = 3 \times 10^{31}$  erg/s. Due to its slow spin, GRO J1744-28 has a large co-rotation radius of 280 km. A mass accretion rate of  $\dot{m} = 5.4 \times 10^{18}$  g/s is needed to reach  $L_c$ . Larger accretion rates are needed to reach the star surface, but such rates distributed over the surface would produce luminosity in excess of the Eddington limit. The fact that the magnetic field is strong enough to funnel a super-Eddington flow to the poles is the likely reason for the type II bursting behavior sometimes seen for this source. In addition to its historical illustration of a propeller effect, this source exemplifies the inverse correlation of spin and magnetic field strength in accreting sources. It requires a weak field to let an accretion disk get close enough to spin up the central object. For this reason we expect Z sources with their stronger B fields to generally spin more slowly than atolls.

The accreting pulsar, **4U0115+63**, with a spin of 0.276 Hz and a magnetic field, derived from its period derivative, of  $1.3 \times 10^{12}$  gauss (yielding  $\mu = 2.9 \times 10^{30}$  gauss cm<sup>3</sup> for a 13 km radius) has been shown [Campana et al. 2002] to exhibit a magnetic propeller effect with a huge luminosity interval from  $L_c = 1.8 \times 10^{33}$  erg/s to  $L_{min} = 9.6 \times 10^{35}$  erg/s.  $L_c$  held steady precisely at the calculated level for a lengthy period before luminosity began increasing. Due to the slow spin of this star, its quiescent luminosity, if ever observed, will be just that emanating from the surface. Its spin-down luminosity will be much too low to be observed.

The atoll source **4U1705-44** has been the subject of a recent study [Barret & Olive 2002] in which a Z track has been displayed in a color-color diagram. Observations labelled as 01 and 06 mark the end points of a spectral state transition for which the luminosity ratio  $L_{min}/L_c = 25.6 \times 10^{36}/6.9 \times 10^{36} = 3.7$  can be found from their Table 2. These yield  $\nu = 470$  Hz and a magnetic moment of  $\mu = 2.5 \times 10^{27}$  gauss cm<sup>3</sup>. The spin-down energy loss rate is  $1.2 \times 10^{37}$  erg/s and the 0.5 - 10 keV quiescent luminosity is estimated to be about  $5 \times 10^{33}$  erg/s. At the apex of the Z track (observation 12), the luminosity was  $2.4 \times 10^{37}$  erg/s (for a distance of 7.4 kpc.); i.e., essentially the same as  $L_{min}$ . Although 4U1705-44 has long been classified as an atoll source, it is not surprising that it displayed the Z track in this outburst as its 0.1 - 200 keV luminosity reached 50% of the Eddington limit.

Considerable attention was paid to reports of a truncated accretion disk for the GBHC, **XTE J1118+480** [McClintock et al 2001] because of the extreme interest in advective accretion flow (ADAF) models for GBHC [Narayan, Garcia & McClintock 1997]. McClintock et al, fit the low state spectrum to a disk blackbody plus power law model and found that the disk inner radius would be about  $35R_{schw}$ , or 720 km for  $7 M_\odot$ . Using this as an estimate of the co-rotation radius we find the spin to be 8 Hz. The corresponding low state luminosity of  $1.2 \times 10^{36}$  erg/s (for  $d = 1.8$  kpc) lets us find a magnetic moment of  $10^{30}$  gauss cm<sup>3</sup>. The calculated spin-down energy loss rate is  $1.5 \times 10^{35}$  erg/s and the quiescent luminosity would be about  $3 \times 10^{31}$  erg/s.

A rare transition to the hard state for **LMC X-3** [Soria, Page & Wu 2002, Boyd et al. 2000] yields an estimate of the mean low state luminosity of  $L_c = 7 \times 10^{36}$  erg/s and the high state luminosity in the same 2 - 10 keV band is approximately  $6 \times 10^{38}$  erg/s at the end of the transition to the soft state. Taking these as  $L_c$  and  $L_{min}$  permits the estimates of spin  $\nu = 16$  Hz and magnetic moment  $\mu = 8.6 \times 10^{29}$  gauss cm<sup>3</sup>, assuming  $7 M_\odot$ . From these we calculate a quiescent luminosity of  $10^{33}$  erg/s.

## Appendix D. The Existence and Stability of Highly Red-shifted MECO

A MECO is, in many ways, more exotic than a black hole with its mere mass and spin. It is equally compact but its surface magnetic field is sufficient to produce bound pairs from the quantum electrodynamic vacuum. This occurs at a threshold that is insensitive to mass, thus MECO can range in mass from the GBHC to AGN. As we shall see, the scaling with mass of the distantly observed magnetic fields,  $B \propto M^{-1/2}$  allows the ratio  $L_c/L_{Edd}$  to also be mass scale invariant [Robertson & Leiter 2004]. The MECO interior magnetic fields are relatively modest. Interior and surface fields differ due to substantial pair drift currents on the MECO surface. In general, plasmas in hydrostatic equilibrium in magnetic and gravitation fields experience

drift currents proportional to  $\mathbf{g} \times \mathbf{B}/B^2$ . The general relativistic generalization of this provides the key to our understanding of the high redshifts of MECO.

The surface temperature and high luminosity to radius ratio (hereafter L/R compactness, see appendix F). of the MECO Eddington limited, timelike, secular collapsing state implies that the plasma is dominated by electron-positron pairs. These are generated by colliding photons due to the optically thick synchrotron luminosity of the intrinsic MECO magnetic field, both within the interior and on the MECO surface. Recall that the surface is well inside the photon orbit and the bulk of the photon outflow from the surface falls back. The existence of the MECO state requires that:

$$L_{Edd}(outflow) \sim L_{Syn}(out) \quad (68)$$

within the MECO and

$$L_{Edd,S}(escape) \sim L_{Syn,S}(escape) \quad (69)$$

at the MECO surface S. Where (see Section 5, Eq. (22))

$$L_{Edd,S}(escape) \sim (4\pi GM_s(\tau)c/\kappa)(1+z_s) \sim 1.3 \times 10^{38}m(1+z_s) \quad (70)$$

$$L_{Syn,S}(escape) \sim L_{Syn,S}(out)/(4/27)(1+z_s)^2 \quad (71)$$

Assuming a temperature near the pair production threshold, the rate of synchrotron photon energy generation in a plasma containing  $N_{\pm}$  electrons and positrons is [Shapiro & Teukolsky 1983]

$$L_{Syn,S}(out) \sim (16e^4/3m_e^2c^3)N_{\pm}B^2(T_9/6)^2 \sim 1.27 \times 10^{-14}N_{\pm}B^2(T_9/6)^2 \text{ erg/s} \quad (72)$$

where  $T_9 = 10^{-9}T$  and  $T_9/6 = kT/m_e c^2$ .

For an Eddington equilibrium, we require the synchrotron generation rate to produce the outflow through the MECO surface. Thus

$$L_{Edd}(out) \sim 1.27 \times 10^{38}m(4(1+z_s)^3/27) \sim 1.27 \times 10^{-14}N_{\pm}B^2(T_9/6)^2 \text{ erg/s} \quad (73)$$

which implies that

$$N_{\pm}B^2 \sim 10^{52}(m/7)(1+z_s)^3(6/T_9)^2 \text{ erg/cm}^3 \quad (74)$$

From Section 6 of Baumgarte & Shapiro [2003], we note that if  $\mu$  is the distantly observed MECO magnetic moment and  $(1+z_s) \gg 1$  is the MECO surface redshift, then the Einstein- Maxwell equations imply that the components of the MECO dipole magnetic field strength, B at distance r are given by

$$B_r = 2F(x)\mu \cos(\theta)/r^3 \quad (75)$$

and

$$B_\theta = G(x)\mu \sin(\theta)/r^3 \quad (76)$$

where  $x = r_s/2R_g$  and

$$F(x) = (-3x^3)(\ln(1 - x^{-1}) + x^{-1}(1 + x^{-1}/2)) \quad (77)$$

$$G(x) = (6x^3)((1 - x^{-1})^{1/2}\ln(1 - x^{-1}) + x^{-1}(1 - x^{-1}/2)(1 - x^{-1})^{-1/2}) \quad (78)$$

Note that for  $r_s \gg 2R_g$ ,  $x \gg 1$  and both  $F(x)$  and  $G(x) \rightarrow 1$ , while as we approach a compact MECO surface where  $(1 + z_s) \gg 1$ , then  $x \rightarrow 1^+$  and

$$F(x) \rightarrow -3\ln(1 - x^{-1}) = -3\ln(1/(1 + z_s)^2) = 6\ln(1 + z_s) \quad (79)$$

and

$$G(x) = 3(1 - x^{-1})^{-1/2} = 3(1 + z_s) \quad (80)$$

Hence the radial component of the magnetic field on the MECO surface is given by

$$B_{r,S+} = 12\ln(1 + z_s)\mu \cos(\theta)/(2R_g)^3 \quad (81)$$

while the poloidal component is given by

$$B_{\theta,S+} = 3\mu(1 + z_s) \sin(\theta)/(2R_g)^3 \quad (82)$$

The interior magnetic dipole fields,  $B'$  in the MECO, which are due to the interior MECO magnetic dipole moment  $\mu(r)$  in the interior will be given by

$$B'_r = 12\mu(r) \cos(\theta) \ln(1 + z)/r^3 \quad (83)$$

and

$$B'_\theta = 6\mu(r) \ln(1 + z) \sin(\theta)/r^3 \quad (84)$$

Thus the expressions for the exterior magnetic field just outside of the MECO surface differ via  $F(x_s)$  and  $G(x_s)$  from those of the interior magnetic field. But these expressions have the following important consequences:

- (a) *The general relativistic structure of the Maxwell-Einstein equations causes the radial and poloidal exterior components of the MECO magnetic dipole fields to undergo redshift effects which are different functions of  $(1 + z_s)$*
- (b) *The radial component  $B_{r,S}$  of the magnetic dipole field is continuous at the MECO surface, but the poloidal component is not.  $B_{\theta,S+}$  is different from  $B'_{\theta,S-}$  at the MECO surface.*

This difference is caused by powerful  $e^\pm$  drift currents that are induced by the strong gravitational field and enhanced by the differing general relativistic dependence on redshift of the poloidal and radial magnetic field components. This is a general relativistic generalization of the fact that a plasma in hydrostatic equilibrium in gravitational and magnetic fields experiences drift currents proportional

to  $\mathbf{g} \times \mathbf{B}/B^2$ . In fact, it is the drift currents that generate the distantly observed magnetic moments seen in MECO-GBHC and MECO-AGN.

The MECO magnetic moment coupling to a surrounding accretion disk will cause it to be a slow rotator. Hence to estimate the strength of the magnetic field just under the surface of the MECO of the GBHC we can use the results obtained for low redshift, slowly rotating compact stellar objects with magnetic fields. The magnetic field strength in the interior of a slowly rotating neutron star of radius  $\sim 10$  km, was shown to be  $\sim 10^{13}$ G [Gupta, Mishra, Mishra & Prasanna 1998]. When scaled to the  $\sim 7M_\odot$  and  $R \sim 2R_g$  size of the MECO, the magnetic fields under the surface can be estimated to be (neglecting latitude angle dependence):

$$B_{r,S^-} \sim (2\mu/(2R_g)^3)6\ln(1+z_s) \sim (10^{13.7} \text{ gauss})/(M/7M_\odot)^{1/2} \quad (85)$$

$$B_{\theta,S^-} \sim (\mu/(2R_g)^3)6\ln(1+z_s) \sim (10^{13.4} \text{ gauss})/(M/7M_\odot)^{1/2} \quad (86)$$

Then from Eq.s (81), (82) and (85), the exterior magnetic fields on the MECO surface S are:

$$B_{r,S^+} = B_{r,S^-} \sim (2\mu/(2R_g)^3)6\ln(1+z_s)\cos(\theta) \sim (10^{13.7} \text{ gauss})\cos(\theta)/(M/7M_\odot)^{1/2} \quad (87)$$

$$B_{\theta,S^+} \sim (\mu/(2R_g)^3)3(1+z_s)\sin(\theta) \quad (88)$$

Using these equations, the magnitude of the surface redshift  $(1+z_s)$  for a MECO can be directly determined by requiring that the strength of the poloidal component of the equipartition magnetic field  $B_{\theta,S}$  on the MECO surface: (a) must be mass scale invariant and, (b) cannot be much larger the quantum electro-dynamically determined maximum value for a NS given by  $B_{\theta,S} \sim 10^{20}$  gauss [Harding, A., 2003]. This is because surface magnetic fields much larger than  $\sim 10^{20}$  gauss would create a spontaneous quantum electrodynamic phase transition associated with the vacuum production of bound pairs on the MECO surface [Zaumen 1976]. This would cause more pairs to be produced than those required by the Eddington balance of the MECO-GBHC surface. This would then cause the MECO-GBHC surface to expand. However the resultant expansion due to this process would reduce the redshift and the surface poloidal magnetic field thus quenching the vacuum production of bound pairs and allowing the MECO-GBHC surface to contract. This stability mechanism on the MECO surface implies that its surface redshift  $(1+z_s)$  can be dynamically determined from the preceding pair of equations. Neglecting the trigonometric functions common to both sides of the equations, the ratio of these external field components in Eq.s (88) and (86), yields

$$3(1+z_s)/[6\ln(1+z_s)] \sim 10^{20}/[10^{13.4}/(m/7)^{1/2}] \quad (89)$$

for which the solution is

$$(1+z_s) \sim 1.5 \times 10^8 (m/7)^{1/2} \quad (90)$$

In addition we obtain

$$\mu/(2R_g)^3 \sim (2.2 \times 10^{11} \text{ gauss})/(m/7)^{1/2} \quad (91)$$

which implies that the average distantly observed intrinsic magnetic moment of the MECO is

$$\mu \sim (2 \times 10^{30} \text{ gauss cm}^3)(m/7)^{5/2} \quad (92)$$

This is in good agreement with our analysis of observations. (See Table 1 and comments near the end of Section 8.)

Using Eq. (74) we can now get a rough estimate of the pair density, by considering the  $N_{\pm}$  to be uniformly distributed over a volume of  $4(1+z_s)\pi(2R_g)^3/3$  and by considering the interior magnetic field to be uniform at  $2.5 \times 10^{13}/(m/7)^{1/2}$  gauss. Hence

$$n_{\pm} = 10^{22}(m/7)^{-3/2}(6/T_9)^2 / \text{cm}^3 \quad (93)$$

which for a GBHC, agrees within a factor of two of the result found for a pair plasma

at  $T = 6 \times 10^9 \text{K}$ . This result for  $n_{\pm}$  implies that surface temperature would increase with increasing mass, however, it only increases by a factor of 10 for  $m = 10^8$ . Since mean MECO densities scale as  $1/m^2$ , one might expect larger density gradients and different ratios of pairs to neutrons and protons in AGN compared to GBHC, which are approximately of nuclear densities.

Azimuthal MECO surface currents are the source of the distantly observed magnetic moment seen in the MECO-GBHC. The magnitude of these surface currents is essentially mass scale invariant and is given by

$$i(S) = (c/4\pi)(\mu/(2R_g)^3)[3(1+z_s)]\sin(\theta) \sim 3.3 \times 10^{26} \text{ amp/cm}^2 \quad (94)$$

total current on GBHC surface, which corresponds to

$$\sim 2 \times 10^{45} e^{\pm} / \text{sec} \quad (95)$$

combined surface e(+ -) flow. Hence (94) and (95) imply that the corresponding drift speeds of electrons and positrons are  $v/c \sim 1$ . This implies that the opposed e(+ -) pairs currents on the MECO surface are moving relativistically and hence will have a very long lifetime before annihilating. This maintains a stable flow of current as required to generate the distantly observed MECO magnetic moments.

The radiation pressure at the outer surface of the MECO is

$$P_{Syn}(out) = L_{Syn}(out)/[4\pi(2R_g)^2 c] \sim 2.7 \times 10^{38}(m/7)^{1/2} \text{ erg/cm}^3 \quad (96)$$

For comparison, the mass-energy density of a MECO is

$$\rho c^2 \sim Mc^2/[(1+z_s)4\pi(2R_g)^3/3] \sim 2 \times 10^{27}/(m/7)^{2.5} \quad (97)$$

which suggests that MECO is radiation dominated and very tightly gravitationally bound. An order of magnitude calculation of binding energy<sup>14</sup> yields  $\sim 1.5Mc^2 \ln(1+z_s)$  for a residual mass,  $M$ . Thus the progenitor of a MECO-GBHC would have a mass of 200-300  $M_\odot$ , and this suggests that they would be among the earliest and most massive stars in the galaxy. A  $10^9 M_\odot$  MECO-AGN could originally consist of  $4 \times 10^{10} M_\odot$ .

## Appendix E. The $\gamma + \gamma \leftrightarrow e^\pm$ Phase Transition and MECO Existence

It is well-known that a spherical volume of radius  $R$  containing a luminosity  $L_\gamma$  of gamma ray photons with energies  $> 1$  MeV,<sup>15</sup> will become optically thick to the  $\gamma + \gamma \leftrightarrow e^\pm$  process when

$$\tau_\pm \sim n_\gamma \sigma_{\gamma\gamma} R \sim 1 \quad (98)$$

and

$$n_\gamma \sim L_\gamma / (2\pi R^2 m_e c^3) \quad (99)$$

is the number density of  $\gamma$ -ray photons with energies  $\sim 1$  MeV,  $L_\gamma$  is the *gamma*-ray luminosity,  $R$  is the radius of the volume, and  $\sigma_{\gamma\gamma}$  is the pair production cross section.

Since  $\sigma_{\gamma\gamma} \sim \sigma_T$  near threshold, it follows that the system becomes optically thick to photon-photon pair production when the numerical value of its compactness parameter  $L_\gamma/R$  is

$$L_\gamma/R \sim 4\pi m_e c^3 / \sigma_T \sim 5 \times 10^{29} \text{ erg/cm-sec} \quad (100)$$

Hence  $\tau_\pm > 1$  will be satisfied for systems with compactness

$$L_\gamma/R > 10^{30} \text{ erg/cm-sec} \quad (101)$$

For an Eddington limited MECO, which has a very large surface redshift  $(1+z) \gg 1$  at  $R \sim 2R_g$ , and taking the proper length and volume into consideration, the optical depth to photon-photon pair production has the very large value

$$\tau_\pm(1+z) \sim (L_{\gamma,30}/R) \sim 10^2 \times (1+z)^3 \gg 1 \text{ erg/cm-sec} \quad (102)$$

Thus the resultant  $\gamma + \gamma \leftrightarrow e^\pm$  phase transition in the MECO magnetic field,  $B_S$ , creates an optically thick pair dominated plasma. Taking the photon escape cone

<sup>14</sup>This has obvious, important consequences for hypernova models of gamma-ray bursters.

<sup>15</sup>1 MeV photons correspond to  $T \sim 10^{10}$  K, which is only slightly beyond the pair threshold, and easily within reach in gravitational collapse.

factor  $\sim 1/(1+z)^2$  into account, the process generates a net outward non-polytropic radiation pressure (see Appendix D)

$$P \sim (1+z)B_S^4 m \quad (103)$$

on the MECO surface. The increase of pressure with redshift is a key feature of the Eddington limited secular balance at  $R \sim 2GM/c^2$ . Thus trapped surfaces, which lead to event horizons, can be prevented from forming. As discussed in Appendix D., the balance is mass scale invariantly stabilized at the threshold of magnetically produced pair breakdown of the vacuum.

## Appendix F - On The Black Hole Kerr-Schild Metric And MECO Vaidya Metric Solutions To the Gravitational Collapse Problem

In discussions with experts in general relativity the validity of our motivation to look for physical alternatives to black holes has been questioned. Our work has been based on the assumption that the preservation of the Strong Principle of Equivalence (SPOE) in Nature implies that metrics with event horizons are non-physical. The objection to this has been based on the well known fact that for massive particles under the action of both gravitational and non-gravitational forces, the timelike nature of the world line of massive particles is preserved. The generally covariant equation of motion for their timelike world lines in spacetime is given by

$$Du^\mu/d\tau = a^\mu = K^\mu \quad (104)$$

Here  $u^\mu$  is the four velocity of the massive particle and  $K^\mu$  is the generally covariant non-gravitational four-vector force which in general relativity is required to obey the dynamic condition

$$K^\mu a_\mu = 0 \quad (105)$$

Then from the above two equations it follows that

$$D(u^\mu u_\mu)/d\tau = 0 \quad (106)$$

which guarantees that [where we have chosen units where  $c=1$  and use the spacetime metric signature (1,-1,-1,-1)]

$$u^\mu u_\mu = 1 \quad (107)$$

From this it follows that in general relativity the timelike invariance of the world line of a massive particle is dynamically preserved for all metric solutions,  $g_{\mu\nu}$ , to the Einstein Equations, including the case of the “event horizon penetrating” Kerr-Schild metric used by most black hole theoreticians in computer simulations of the

black hole collapse of a radially infalling massive particle or fluid. On the basis of the above facts it is then argued that there is no reason to look for physical alternatives to black holes and that the assumption that the preservation of the Strong Principle of Equivalence (SPOE) in Nature implies that metrics with event horizons are non-physical, is in error.

However we will now show that above arguments, which are based on the four velocity  $u^\mu$  alone, are not valid. This is because relativists who come to this conclusion in this manner are making the mistake of ignoring the fact that in addition to the four velocity  $u^\mu$  there exists another important quantity called the “physical 3-velocity” which must also be considered as well. Physically speaking, the magnitude of the physical 3-velocity is seen by an observer at rest as being equal to the speed of the co-moving observer who is moving along with the collapsing massive particle or fluid. If we consider the case of a radially infalling massive particle or fluid undergoing gravitational collapse it can be shown that the radial component of the physical 3-velocity is given by

$$V^r = c \frac{[(g_{0r}g_{0r} - g_{rr}g_{00})v^r v^r]^{1/2}}{|(g_{00} + g_{0r}v^r)|} \quad (108)$$

where  $v^r = dr/d\tau$  is the radial coordinate velocity of the massive particle or fluid (See Landau and Lifshitz., 1975 “classical Theory of Fields”, 4th Ed, Pergamon Press pg 248-252).

From the above formula for the radial component of the physical 3-velocity of the co-moving observer  $V^r$  we see that for metrics which have the property that  $g_{00} \rightarrow 0$  in some region of spacetime (i.e. the property associated with the existence of an event horizon for the non-rotating metrics associated with the radial infall of matter) the physical radial velocity  $V^r$  of the co-moving frame of the massive particle or fluid becomes equal to the speed of light as the massive particle or fluid crosses the event horizon.

Hence even though the timelike property  $u^\mu u_\mu = 1$  is preserved for a massive particle or fluid crossing the event horizon of the Kerr-Schild metric where  $g_{00} \rightarrow 0$  occurs, a local special relativistic connection between the co-moving frame of the radially infalling massive particle or fluid and a stationary observer can no longer be made. Since the Strong Principle Of Equivalence (SPOE) requires that Special Relativity must hold locally at all points in spacetime, the breakdown at the event horizon, of the local special relativistic connection between the co-moving observer frame and a stationary observer frame for a particle crossing the event horizon, represents a violation of the SPOE. Hence we have shown that by considering both the four velocity and the “physical 3-velocity of the co-moving observer” there is motivation to look for physical alternatives to black holes. In fact in this context logical arguments can be consistently made which show that Black Holes with non-zero mass cannot exist in Nature (Mitra, A., 2000, 2002, 2005, 2006).

Based on the above arguments, the SPOE preserving requirement that the co-moving observer frame for a massive collapsing fluid must always be able to be

connected to a stationary observer by special relativistic transformations with a physical 3-speed which is less than the speed of light, was taken seriously in our work. In the literature the requirement that the SPOE must be preserved everywhere in spacetime for the timelike worldlines of massive particles or fluids under the influence of both gravitational and non-gravitational forces goes under the technical name of “timelike worldline completeness”.

Based on this idea we have found that preservation of the SPOE in Nature can be accomplished only if there exist non-gravitational components in the energy-momentum tensor on the right hand side of the Einstein equation that physically guarantee the preservation of the SPOE. It was in this alternative context that the general relativistic MECO solutions to the Einstein-Maxwell equations emerged, as was shown in the three previously published papers of Robertson and Leiter and developed in more detail in Appendix 1-10 in this paper. There it was shown that for a collapsing body, the structure and radiation transfer properties of the energy-momentum tensor on the right hand side of the Einstein field equations, could describe a collapsing radiating object which contained equipartition magnetic fields that generated a highly redshifted Eddington limited secular collapse process. This collapse process was shown to satisfy the SPOE requirement of Timelike Worldline Completeness by dynamically preventing trapped surfaces, that lead to event horizons, from forming.

More specifically in Appendix A-E it was shown that, by using the Einstein-Maxwell Equations and Quantum Electrodynamics in the context of General Relativistic plasma astrophysics, it was possible to virtually stop and maintain a slow, (many Hubble times!) steady collapse of a compact physical plasma object outside of its Schwarzschild radius. The non-gravitational force was Compton photon pressure generated by synchrotron radiation from an intrinsic equipartition magnetic dipole field contained within the compact object. The rate of collapse is controlled by radiation at the local Eddington limit, but from a highly redshifted surface. In Appendix D it was shown that general relativistic surface drift currents within a pair plasma at the MECO surface can generate the required magnetic fields. In Appendix D the equatorial poloidal magnetic field associated with a locally Eddington limited secular rate of collapse of the exterior surface was shown to be strong enough to spontaneously create bound electron-positron pairs in the surface plasma of the MECO. In the context of the MECO highly redshifted Eddington limited balance, the action of this QED process was shown to be sufficient to stabilize the collapse rate of the MECO surface.

For the case of hot collapsing radiating matter associated with the MECO, the corresponding exterior solution to the Einstein equation was shown to be described by the time dependent Vaidya metric. No coordinate transformation between MECO Vaidya metric and the Black Hole Kerr-Schild metric exists. Since the highly redshifted MECO Vaidya metric solutions preserve the SPOE and they do not have event horizons, they can also contain a slowly rotating intrinsic magnetic dipole mo-

ment. These magnetic moments have observable effects if such MECO exist at the centers of galactic black hole candidates and AGN. In recent work (Schild, Robertson & Leiter 2005) we have found observational evidence of the physical effects of such intrinsic magnetic dipole fields in the central compact object in the Quasar Q0957+561. It is important to note that these physical effects cannot be explained in terms of standard Black Hole models using Kerr-Schild metric driven GRMHD calculations, since these calculations generate unphysical “split magnetic monopole fields” that cannot explain the details of the intrinsic structure in Q0957+561 that our observations have found.

We reiterate that the Kerr-Schild metric used by most relativists is not relevant to the work done in this paper, because the collapsing radiating MECO solution to the Einstein equation is described by the time dependent radiating Vaidya metric, and there is no coordinate transformation between them. Therefore we found that we had to turn to alternate MECO Vaidya metric solutions to the Einstein-Maxwell equations which feature the intrinsic magnetic dipole fields implied by the observations.

### Acknowledgements

We thank Abhas Mitra for seminal ideas, helpful comments and criticisms and many discussions of issues related to gravitational collapse. Useful information has been generously provided by Mike Church, Heino Falcke, Elena Gallo, Thomas Maccarone and Jeff McClintock.

### References

- Abramowicz, M., Kluzniak, W. & Lasota, J-P, 2002 *A&A* **396**, L31
- Abrams, L. S. , 1979 *Phys. Rev. D* **20**, 2474
- Abrams, L. S. , 1989 *Can J. Phys.* **67**, 919, gr-qc/0102051
- Anderson, H. L. , 1989 in ‘A Physicists Desk Reference’, Ed. AIP, p68
- Arons, J. et al. 1984 in ‘High Energy Transients in Astrophysics’, AIP Conf. Proc. 115, 215, Ed. S. Woosley, Santa Cruz, CA
- Barret, D. & Olive, J-F. , 2002 *ApJ* **576**, 391
- Belloni, T., Mendez, M., King, A., van der Klis, M. & van Paradijs, J. 1997 *ApJ* **488**, L109
- Baumgarte, T. & Shapiro, S. 2003 *ApJ* **585**, 930
- Bhattacharya D. , & Srinivasan, G., 1995 in ‘X-Ray Binaries’, eds W. Lewin, J. van Paradijs & E. van den Heuvel, Cambridge Univ. Press

- Bisnovatyi-Kogan, G. & Lovelace, R. 2000 *APJ* **529**, 978
- Boyd, P. et al. 2000 *ApJ* **542**, L127
- Brazier, K. et al. , 1990 *ApJ* **350**, 745
- Burderi, L., et al. 2002 *ApJ* **574**, 930
- Campana, S. et al. , 2002 *ApJ* **580**, 389
- Campana, S. et al. , 1998 *A&A Rev.* **8**, 279
- Chakrabarty, D. et al. , 2003 *Nature* **424**, 42
- Chou & Tajima 1999 *ApJ* **513**, 401
- Church, M.J. 2001 in Advances in Space Research, 33rd Cospar Scientific Assembly, Warsaw, Poland July 2000 astro-ph/0012411
- Church, M. & Balucinska-Church, M. 2001 *A&A* **369**, 915
- Coburn, W. & Boggs, S., 2003 *Nature* **423**, 415
- Corbel, S. & Fender, R. 2002 *ApJ* **573**, L35
- Cui, W. 1997 *ApJ* **482**, L163
- Done, C. & Życki, P. 1999 *MNRAS* **305**, 457
- Gallo, E., Fender, R., Pooley, G. , 2003 *MNRAS*, **344**, 60
- Galloway, D., Chakrabarty, D., Morgan, E., & Remillard, R. 2002 *ApJL* **576**, 137
- Garcia, M. et al .. 2001 *ApJ* **553**, L47
- Ghosh, P. & Lamb, F. 1992 in X-Ray Binaries and Recycled Pulsars, Ed. E. van den Huevel and S. Rappaport, Kluwer
- Gliozzi, M., Bodo, G. & Ghisellini, G. 1999 *MNRAS* **303**, L37
- Gnedin, Y. et al. , 2003 *Astrophys. Sp. Sci* accepted, astro-ph/0304158
- Goodson, A., Bohm, K. & Winglee, R. 1999 *ApJ* **534**, 142
- Gupta, A., Mishra, A., Mishra, H., & Prasanna, A.R. , 1998, 'Classical and Quantum Gravity', 15, 3131
- Harding, A. , 2003, Invited talk at Pulsars, AXPs and SGRs Observed with BeppoSAX and Other Observatories, Marsala, Sicily, Sept. 2002 astro-ph/0304120.
- Hawley, J., Balbus, S. & Winters, W. , 1999 *ApJ* **518**, 394
- Hernandez Jr., W.C. & Misner, C.W., 1966 *ApJ.* **143**, 452

- Iaria, R. et al. 2001 *ApJ* **547**, 412
- Ibrahim, A., Swank, J. & Parke, W. , 2003 *ApJ* **584**, L17
- Ilarianov, A. & Sunyaev, R. 1975 *A&A* **39**, 185
- Kato, Y., Hayashi, M., Matsumoto, R. 2004 *ApJ* in press astro-ph/0308437
- Kippenhahn, R. & Weigert, A. 1990 'Stellar Structure and Evolution' Springer-Verlag, Berlin Heidelberg New York
- Kluzniak, W. & Ruderman, M , 1998 *ApJL* **505**, 113
- Landau, L.D. & Lifshitz, E. M. , 1975 'Classical Theory of Fields', 4th Ed, Pergamon Press p248-252
- Landau, L. & Lifshitz, E. 1958 'Statistical Physics', Pergamon Press LTD, London
- Leiter, D. & Robertson, S. , 2003 *Found Phys. Lett.* **16** 143
- Lindquist, R. W., Schwartz, R. A. & Misner , C. W. 1965 *Phys. Rev.*, **137B**, 1364.
- Lindquist, R. W. , 1966 *Annals of Physics*, **37**, 487
- Livio, M., Ogilvie, G. & Pringle, J. 1999 *ApJ* **512**, 100
- Maccarone, T., Gallo, E., Fender, R. 2003 *MNRAS* **345**, L19
- Markoff, S., Falcke H., & Fender, R. 2001 *A&AL* **372**, 25
- Markoff, S., Nowak, M., Corbel, S., Fender, R., Falcke, H. , 2003 *New Astron. Rev.* **47**, 491
- Markwardt, C. , et al. 2002 *ApJL* **575**, 21
- Matt, S., Goodson, A., Winglee, R. , Böhm, K. 2002 *ApJ* **574**, 232
- Mauche, C. W. , 2002 *ApJ* **580**,423
- McClintock, J. et al. , 2001 *ApJ* **556**, 42
- Merloni, A., Fabian, A. , 2002 *MNRAS*, **332**, 165
- Merloni, A., Heinz, S., Di Matteo, T. , 2003 *MNRAS*, **345**, 1057
- Miller, J. et al. , 2003 *ApJL*, **583**, 99
- Misner, C. W. 1965 *Phys. Rev.*, **137B**, 1360
- Misner, C. , Thorne, K. & Wheeler, J. 1973 'Gravitation', Freeman, San Francisco, California
- Mitra, A. 1998 *ApJ* **499**, 385

- Mitra, A. 2000 *Found. Phys. Lett.* **13**, 543
- Mitra, A. 2002 *Found. Phys. Lett.* **15**, 439
- Mitra, A. 2005, Talk given at the 29th International Cosmic Ray Conference in Pune India, astro-ph/0506183
- Mitra, A. 2005 astro-ph/0512006
- Mitra, A. in press 2006 in 'Focus On Black Hole Research', ed. P.V. Kreitler, Nova Science Publishers, Inc. ISBN 1-59454-460-3, novapublishers.com)
- Mitra, A. 2006 *MNRAS Letters* in press, gr-qc/0601025
- Muno, M., Remillard, R. & Chakrabarty, D. 2002 *ApJ* **568**, L35
- Narayan, R., Garcia, M., McClintock, J. , 1997 *ApJ*. **478**, L79
- Orosz, J., Remillard, R., Bailyn, C. & McClintock, J. 1997 *ApJ* **478**, L83
- Paragi, Z., et al. 2002 Talk presented at the 4th Microquasar Workshop, Cargese, Corsica May 27-31 astro-ph/0208125
- Pelletier, G. & Marcowith, A. , 1998 *ApJ* **502**, 598
- Possenti, A., Cerutti, R., Colpi, M., & Mereghetti, S. 2002 *A&A* **387**, 993
- Punsly, B. 1998 *ApJ* **498**, 640
- Psaltis, D., Belloni, T. , & van der Klis, M., 1999 *ApJ* **520**,262
- Reid, M. et al. , 2003 *ApJ* **587**, 208
- Robertson, S. & Leiter, D. 2002 *ApJ*, **565**, 447
- Robertson, S., Leiter, D. 2003 *ApJ*, **596**, L203
- Robertson, S., Leiter, D. 2004 *MNRAS* **350**, 1391
- Robertson, S., and Leiter, D. 2005 'The Magnetospheric Eternally Collapsing Object (MECO) Model of Galactic Black Hole Candidates and Active Galactic Nuclei', pp 1-45 (in New Developments in Black Hole Research, ed. P.V.Kreitler, Nova Science Publishers, Inc. ISBN 1-59454-460-3, novapublishers.com)
- Schild, R., Leiter, D. & Robertson submitted to *AJ* astro-ph/0505518
- Shapiro, S. & Teukolsky, S. 1983 in 'Black Holes, White Dwarfs & Neutron Stars', John Wiley & Sons, Inc., New York
- Soria, R., Page, M. & Wu, K. 2002 in Proceedings of the Symposium 'New Visions of the X-Ray Universe in the XMM-Newton & Chandra Era', Nov. 2001, ESTEC, the Netherlands, astro-ph/0202015

- Stella, L., White, N. & Rosner, R. 1986 *ApJ* **308**, 669
- Strohmayer, T. & Markwardt, C. , 2002 *ApJ* **577**, 337
- Sunyaev, R. , 1990 Soviet Astron. Lett. 16, 59
- Tanaka, Y.& Lewin, W. , 1995 in 'Black-hole binaries' in X-ray Binaries ed. W. Lewin, J. van Paradijs& E. van den Heuvel (Cambridge: Cambridge Univ. Press)
- Tanaka, Y. & Shibazaki, N. , 1996 *ARA&A*, **34**, 607
- Thorne, K. , 1965 *Phys. Rev*, **138**, B251
- Titarchuk, L. & Wood, K., 2002 *ApJL* **577**, 23
- Uzdensky, D. , 2002 *ApJ* **572**, 432
- Vadawale, S., Rao, A. & Chakrabarti, S. 2001 *A&A* **372**, 793V
- van der Klis, M. 1994 *ApJS* **92**, 511
- Warner, B. & Woudt, P. , 2003 in ASP Conf. Series, Ed. M. Cuppi and S. Vriellmann astro-ph/0301168
- Wheeler, J. & Ciufolini, I. , 1995 in 'Gravitation And Inertia' Princeton Univ. Press, 41 William St., Princeton, New Jersey
- White, N.& Marshall, F. 1984, *ApJ*. **281**, 354
- Wilson, C. & Done, C. 2001 *MNRAS* **325**, 167
- Zaumen, W. T. , 1976 *ApJ*, **210**, 776
- Zhang, W., Yu, W. & Zhang, S. 1998 *ApJ* **494**, L71
- Życki, P., Done, C. and Smith , D. 1997a in AIP Conf. Proc. 431, Accretion Processes in Astrophysical Systems: Some Like It Hot, Ed. S. S. Holt & T. R. Kallman (New York, AIP), 319
- Życki, P., Done, C. and Smith 1997b *ApJ* **488**, L113